



Triassic alkaline magmatism of the Hawasina Nappes: Post-breakup melting of the Oman lithospheric mantle modified by the Permian Neotethyan Plume

François Chauvet, Henriette Lapierre, René Maury, Delphine Bosch,
Christophe Basile, Joseph Cotten, Pierre Brunet, Sylvain Campillo

► To cite this version:

François Chauvet, Henriette Lapierre, René Maury, Delphine Bosch, Christophe Basile, et al..
Triassic alkaline magmatism of the Hawasina Nappes: Post-breakup melting of the Oman litho-
spheric mantle modified by the Permian Neotethyan Plume. *Lithos*, 2011, 122 (1-2), pp.122-136.
10.1016/j.lithos.2010.12.006 . insu-00559080

HAL Id: insu-00559080

<https://hal-insu.archives-ouvertes.fr/insu-00559080>

Submitted on 18 Mar 2011

HAL is a multi-disciplinary open access archive for the deposit and dissemination of scientific research documents, whether they are published or not. The documents may come from teaching and research institutions in France or abroad, or from public or private research centers.

L'archive ouverte pluridisciplinaire **HAL**, est destinée au dépôt et à la diffusion de documents scientifiques de niveau recherche, publiés ou non, émanant des établissements d'enseignement et de recherche français ou étrangers, des laboratoires publics ou privés.

Triassic alkaline magmatism of the Hawasina Nappes: post-breakup melting of the Oman lithospheric mantle modified by the Permian Neotethyan Plume.

François Chauvet ^{a, b*}, Henriette Lapierre ^{b†}, René C. Maury ^c, Delphine Bosch ^d, Christophe Basile ^b, Joseph Cotten ^c, Pierre Brunet ^e, Sylvain Campillo ^b

^a *Université des Sciences de Nantes; CNRS-UMR 6112; Laboratoire de Planétologie et Géodynamique de Nantes, 2 rue de la Houssinière, BP 92208, 44322 Nantes Cedex 3, France.*

^b *Université Joseph Fourier; CNRS-UMR 5025; Laboratoire de Géodynamique des Chaînes Alpines; Observatoire des Sciences de l'Univers de Grenoble, Maison des Géosciences 1381 rue de la Piscine, 38400 Saint Martin d'Hères, France.*

^c *Université Européenne de Bretagne, Université de Brest; CNRS; UMR 6538 Domaines Océaniques; Institut Universitaire Européen de la Mer, Place N. Copernic, 29280 Plouzané, France.*

^d *Université de Montpellier II; CNRS; UMR 5243 Géosciences Montpellier, Equipe Manteau-Noyau; Place E. Bataillon, 34095 Montpellier Cedex 05, France.*

^e *Université Paul Sabatier; CNRS; UMR 5563 Laboratoire Mécanismes de Transfert en Géologie; Observatoire Midi-Pyrénées, 14 avenue E. Belin, 31400 Toulouse, France.*

* Corresponding author. Tel.: (33)251125474; fax: (33)251125268.

E-mail address: francois.chauvet@univ-nantes.fr

ABSTRACT

Middle to Late Triassic lavas were sampled within three tectonostratigraphic groups of the Hawasina Nappes in the Oman Mountains. They are predominantly alkali basalts and trachybasalts, associated with minor sub-alkaline basalts, trachyandesites, trachytes and rhyolites. Their major, trace elements and Nd-Pb isotopic compositions are very similar to those of the Permian plume-related high-Ti basalts which also occur in the Hawasina Nappes. The Triassic lavas derive from low-degree melting of an enriched OIB-type mantle source, characterized by $\epsilon\text{Nd}_i = 0.3\text{--}5.3$ and $(^{206}\text{Pb}/^{204}\text{Pb})_i = 16.96\text{--}19.31$ (for $t = 230$ My). With time, melting depths decreased from the garnet + spinel to the spinel lherzolite facies and the degree of melting increased. The oldest are distinguished from the others by unradiogenic Nd and Pb signatures, with $\epsilon\text{Nd}_i = -4.5$ to -1.2 and $(^{206}\text{Pb}/^{204}\text{Pb})_i = 16.35\text{--}17.08$, which we attribute to their contamination by Arabo-Nubian lower crust. The lavas likely derived from the Oman lithospheric mantle, the original DMM-HIMU signature of which was overprinted during its pervasive metasomatism by the Permian plume-related melts. We suggest that these lavas were emplaced during post-breakup decompression-triggered melting in the Middle Triassic during global kinematic reorganization of the Tethyan realm.

40 **1. Introduction**

41

42 Petrologic and geochemical studies of ancient oceanic crust and continental margins can
 43 be used to reconstruct the dynamics of past rifting and oceanization processes. The Middle
 44 Permian opening of the Neotethyan Ocean (Besse et al., 1998) separated Gondwana from
 45 Cimmerian continental blocks (Ricou, 1994; Stampfli and Borel, 2002). It led to the formation
 46 of passive continental margins south of the Neotethys Ocean, i.e. on the northern edges of the
 47 Australian, Indian, Arabian and African shields. Cretaceous to Neogene convergence between
 48 Laurasia and Gondwana (Stampfli and Borel, 2002) then led to the disappearance of
 49 Neotethyan oceanic crust. Fragments of its southern margins were incorporated into Alpine
 50 collisional belts in the Himalayas, Oman, Zagros, Syria, Cyprus, Turkey and Greece
 51 (Coleman, 1981, Fig. 1a).

52 These inverted margin fragments carry remnants of successive magmatic episodes, which
 53 can be used to constrain the formation and development stages of the southern Neotethyan
 54 margin. For instance, Middle Permian flood basalts are widespread in NW Indian (Panjal
 55 Traps) and Oman (Saih Hatat and Hawasina nappes Fig. 1a). Their plume-related
 56 geochemical features suggest that the breakup of Gondwana was associated with the
 57 emplacement of an intraplate volcanic province and associated volcanic-type margins
 58 (Garzanti et al., 1999; Maury et al., 2003; Lapierre et al., 2004; Chauvet et al., 2008).
 59 Younger (post-breakup) volcanic sequences are generally tectonically associated with
 60 Tethyan ophiolitic nappes, from the Himalayas to the eastern Mediterranean (Fig. 1a). Within
 61 these nappes, volcanic rocks are stratigraphically associated with late Middle to Late Triassic
 62 pelagic sediments and/or reef limestones. In the Oman Mountains, these Triassic post-breakup
 63 volcanic series have been considered as tectonically inverted intra-oceanic plateaus or
 64 seamounts (Glennie et al., 1974; Searle et al., 1980; Searle and Graham, 1982; Robertson and
 65 Searle, 1990; Stampfli et al., 1991; Pillevuit, 1993; Pillevuit et al., 1997), as well as their
 66 equivalents in the Himalayas (Ahmad et al., 1996; Robertson, 1998; Corfield et al. 1999) and
 67 Mediterranean sequences (Syria: Al Riyami and Robertson, 2002; Cyprus: Lapierre et al.,
 68 2007; Chan et al., 2008; Turkey: Maury et al., 2008; Greece: Monjoie et al., 2008).
 69 Alternatively, the Oman Triassic lavas have been interpreted as remnants of a second rifting
 70 episode of the Arabian continental margin (Lippard et al., 1986; Béchenec et al., 1988, 1990,
 71 1991).

72 A new petrologic and geochemical investigation (major and trace elements and Nd, Pb
 73 isotopes) of Middle to Late Triassic lavas from the allochthonous units of the Oman
 74 Mountains allows us to address these two hypotheses.

2. Geological setting

The Arabian continental margin of the Neotethys ocean formed during Permo-Triassic times (Béchenec et al., 1988; Robertson and Searle, 1990). Reconstructions of this margin (Glennie et al., 1974; Béchenec, 1987) suggest the occurrence of a continental platform (Saiq Fm.), a continental slope (Sumeini Group), and basinal environments (Hawasina units). In the Oman Mountains, remnants of several basins are exposed in the Hawasina Nappes, which are sandwiched between the autochthonous Arabian platform and the Semail ophiolitic nappe (Fig. 1b; Bernouilli and Weissert, 1987; Béchenec et al., 1988). They include Middle Permian (Murghabian) to Late Cretaceous sedimentary and volcanic units.

Béchenec (1987) and Béchenec et al. (1988, 1990, 1993) distinguished four tectonostratigraphic groups within the Hawasina Nappes tectonic pile (Fig. 1c,d). From the base to the top, they are the Hamrat Duru, Al Aridh, Kawr and Umar Groups (Fig. 1d). These groups were emplaced either in proximal (Hamrat Duru) or distal (Umar) pelagic basins, in a trench or slope (Al Aridh) or as an isolated carbonate platform (Kawr). While the Hamrat Duru basin appeared during the Middle Permian major rifting event, the three others (Al Aridh, Kawr and Umar Groups) formed during Middle to Late Triassic (de Wever et al., 1990). Because they are mainly found within tectonic slices, the remnants of the Hawasina Triassic carbonate platform were also named Oman Exotics (Glennie et al., 1974; Searle and Graham, 1982; Robertson and Searle, 1990) and the Umar Group volcanics correspond to the Haybi Volcanics of Searle et al. (1980). The latter authors performed geochemical analyses on a Permian and Triassic sample set coming from the northern part of the Oman Mountains.

Middle to Late Triassic volcanic sequences (ca. 10 to 100 m-thick) and associated magmatic intrusions occur (i) below and within the pelagic sediments of the Umar Group (Sinni Fm.); (ii) below and within the Kawr platform carbonates (Misfah Fm.); (iii) below the Al Aridh Group slope/trench deposits (Sayfam Fm.); and finally (iv) within the pelagic deposits of the Hamrat Duru Group (Matbat Fm.). Synsedimentary megabreccias intercalated within the proximal successions of the Hawasina Nappes (Watts, 1990; Pillevuit, 1993) suggest contemporaneous tectonic activity. This Middle to Late Triassic tectono-magmatic event occurred 30 to 40 My after the Middle Permian opening of Neotethys (Béchenec, 1987; Pillevuit, 1993; Baud et al., 2001).

3. Sampling and petrography

In this study, lavas from the Umar and Kawr Groups were sampled in the central part of the Oman Mountains, near the western termination of the Jabal Akhdar anticline (Al Qurti and Misfah localities, Fig. 1c,d). Additional samples were collected from three other Umar sites (Sinni, Sayjah and Aqil villages, Fig. 1c). The Al Aridh Group volcanics were sampled on the SW and NW flanks of the Jabal Buwaydah. Coeval volcanics from Hamrat Duru Group were not studied.

3.1. The Umar Group

The Umar Group is directly overthrust by the Semail ophiolite (Fig. 1c,d). Its Triassic succession includes three lithofacies (UmV₁₋₃, Béchenec, 1987; Beurrier et al., 1986) which are well exposed as a succession of tectonic slices in the Al Qurti section (Appendix A). The 15 samples collected along this section exhibit the largest petrologic diversity of our suite, with, from base to top, basalts, trachyandesites, trachytes and rhyolites. The basal unit (UmV₁) corresponds to a 100 m thick succession of basaltic pillow-lavas, often tubular and dominated by subaphyric to porphyritic vesicular basalts with dispersed clinopyroxene phenocrysts (Om04-10, -11, -12). The second unit (UmV₂) includes basaltic flows capped with pelagic sediments (Om04-18, -19) and trachyandesitic pillowed lavas (Om04-17, -24, -27), successively overlain by hyaloclastites and volcanogenic debris flows. The latter contain rhyolitic lava blocks with plagioclase (Om04-29) and quartz grains (Om04-34, -35). The third unit (UmV₃), emplaced between the Kawr and Umar Groups, corresponds to columnar-jointed plugs showing trachytic textures with Na-rich plagioclase microcrysts and rare biotite phenocrysts (Om04-37, -38).

3.2. The Kawr Group

In the Hawasina nappes, the Kawr Group outcrops mainly south of the western termination of Jabal Akhdar anticline, in several mountains capped by high carbonate cliffs (Jabal Misht, Jabal Misfah, Jabal Kawr, and Jabal Ghul; Fig. 1c). Its stratigraphy (Béchenec, 1987; Pillevuit, 1993) has been defined on the northern and eastern slopes of Jabal Misfah (Appendix A). A 50 m thick basal volcanic unit, dated Ladinian-Carnian (Pillevuit, 1993) is made up of massive and pillowed basaltic flows, hyaloclastites and tuffites. These volcanics are successively overlain by Ladinian-Carnian to Rhaetian marly limestones, by thick and massive platform limestones crosscut by numerous basaltic dikes and sills, and finally by Jurassic to Cretaceous pelagic deposits. Among the 23 samples (Appendix A) collected from the Kawr Group, 11 come from the basal volcanic unit and 12 from the dykes and intrusive bodies. The basal flows, as well as the sills and dykes, show aphyric (Om04-52 and -54),

145 microlitic (Om04-56, -59, -66), or highly porphyritic textures with abundant clinopyroxene
146 phenocrysts (Om04-55, -57, -58).

148 3.3 The Al Aridh Group

149 The Al Aridh Group mainly outcrops along the southern flank of the Oman Mountains
150 (Fig. 1c). It includes a basal volcanic sequence overlain by breccia horizons dated
151 Middle/Late Triassic to Santonian (Béchenec et al., 1993). Seven samples were collected
152 from two sites in Jabal Buwaydah, located south of the Jabal Kawr (Fig. 1c). The first one
153 (“Buwaydah 1” in Fig. 1c) exposes a 40 m thick sequence of sills and massive flows,
154 intercalated with basaltic pillows and overlain by a trachyandesitic flow. In the second
155 locality (“Buwaydah 2” in Fig. 1c), the 150 m thick volcanic succession is capped by cherts
156 and pelagic limestones dated Carnian to basal Norian (de Wever et al., 1990). The Al Aridh
157 Group samples are porphyritic basaltic to trachyandesitic lavas with serpentinized olivine,
158 fresh clinopyroxene and Fe-Ti oxides phenocrysts.

160 4. Geochemical data

162 4.1. Analytical methods

163 Sixty one samples (31 from the Umar, 23 from the Kawr and 7 from Al Aridh Group)
164 were selected for petrographic and geochemical analysis. These rocks were pulverized in an
165 agate mill and analysed using methods similar to those described in previous papers (see
166 Chauvet et al., 2008 and references therein). Major elements and a set of trace elements
167 (shown in italics in Table 1 and Appendix B) were determined by inductively coupled
168 plasma-atomic emission spectrometry (ICP-AES) at the Université de Bretagne Occidentale
169 in Brest, following the procedures of Cotten et al. (1995) and using international standards for
170 calibration tests (AC-E, BE-N, JB-2, PM-S, WS-E). Rb contents were measured by flame
171 atomic emission spectroscopy. Relative standard deviations were ~ 1 % for SiO₂ and 2 % for
172 other major elements except P₂O₅ and MnO (0.01%), and ~ 5 % for trace elements.
173 Additional trace element contents (Table 1) were measured by ICP-MS at the Université
174 Joseph Fourier in Grenoble on 45 samples (27 from Umar, 14 from Kawr and 4 from Al
175 Aridh), using the procedures of Barrat et al. (1996) and BHVO-2, BEN and BR-24 standards.
176 Analytical errors were less than 3 % for trace elements except Cs (<5%).

177 Isotopic Nd and Pb data (Table 2) were corrected for *in situ* decay using an average age of
178 230 Ma (Ladinian-Carnian). All the Hawasina samples were leached twice in 6N HCl during
179 30 minutes at 100°C before acid digestion and Nd and Pb chemical separation in order to
180 avoid or minimize alteration effects (see below). Nd (semi-dynamic acquisition) isotopic

ratios of 21 samples labelled Om-29 to Om-207 were measured at LMTG, Université Paul Sabatier, Toulouse, on a Finnigan MAT 261 multicollector mass spectrometer using the analytical procedures of Lapierre et al. (1997). Results on standards yielded $^{143}\text{Nd}/^{144}\text{Nd} = 0.511958 \pm 34$ ($n = 6$) for the Neodymium Rennes Standard (Chauvel and Blichert-Toft, 2001). $^{143}\text{Nd}/^{144}\text{Nd}$ measured ratios were normalized for mass fractionation relative to $^{146}\text{Nd}/^{144}\text{Nd} = 0.7219$. In addition, 39 samples were selected for lead separation and leached with 6N tridistilled HCl during 30 minutes at 85°C before acid digestion (36-48 hours in ultrapure HF and HNO₃ acids). Pb blanks were less than 40 pg. Lead isotopes and Nd isotopic ratios of samples labelled “Om04-” and “Om05-” and Pb were measured on a Nu-plasma 500 multicollector magnetic-sector ICP-MS at the Ecole Normale Supérieure in Lyon. Details about chemical separations and isotope analytical measurements including reproducibility, accuracy and standards, can be found in Bosch et al. (2008) and references therein.

4.2. Alteration and sample selection

Ancient lavas are altered, a process that disturbs their major and trace element patterns and complicates calculation of initial isotopic ratios. Although our samples were carefully selected in the field, none of them is devoid of post-magmatic minerals and they often display numerous fractures filled with calcite, iron oxides and/or smectites. Pillow groundmass and vesicles contain variable amounts of calcite, zeolites and clays. In addition, the occasional presence of chlorite suggests that some Hawasina basin lavas underwent hydrothermal alteration or low-grade greenschist metamorphic conditions.

The loss on ignition (LOI) values of analyzed samples range from 2 to 13 wt.%, with more than half of them below 6 wt.% (Table 1 and Appendix B). Major elements analyses have been recalculated to 100% (volatile-free basis). The highest LOI values (> 10 wt.%) were measured in the Umar Group vesicular pillow lavas and in the Kawr Group intrusions, the groundmass of which is totally replaced by zeolites and calcite. Despite the high LOI values of the studied samples, SiO₂, MgO, Al₂O₃, P₂O₅ and TiO₂ contents variations from mafic to felsic lavas are relatively regular, and consistent with the petrographic (thin section) features of these rocks. In contrast, the large and erratic variations of CaO and Na₂O/K₂O at a given SiO₂ or MgO content (Table 1, Appendix B) or at a given “immobile” trace element content (e.g. Zr) suggests the mobility of alkaline and alkaline earth elements during alteration and/or recrystallization.

The analyzed samples display rather regular chondrite- and primitive mantle-normalized trace element patterns (Appendix C), with the exception of large ion lithophile elements (LILE). For instance, Rb, Ba and Sr exhibit strong negative or positive anomalies in

multielement patterns which could have been generated either by their remobilization during post-magmatic processes (hydrothermalism and/or weathering) or by contamination processes during the evolution of their parental magmas. Nevertheless, the erratic behavior of Ca, Na, K and LILE is particularly obvious for samples showing the highest LOI and/or the largest amount of post-magmatic minerals. Thus, no attempt was made to use them to constrain igneous processes. In contrast, La, Nd, Sm, U and Pb correlate well with Th (Appendix D) and with high field strength elements (HFSE, not shown in Appendix D). These features suggest that the REE and HFSE contents of the studied samples, as well as their Pb and Nd isotopic compositions, represent reliable tools to investigate the petrogenesis of Hawasina Triassic lavas.

Sample selection for Pb isotopic analyses (39 samples out of the 54 analyzed for Nd, Appendix D) was aimed to eliminate the most altered samples and to account for the observed petrologic and geochemical variations. In the Pb and U *versus* Th diagrams (Appendix D), a majority of analyzed samples display Th/U and Th/Pb ratios close to the OIB mean values. However, despite a drastic sample selection, significant dispersions of Pb and U concentrations are still observed, particularly for Om-49 and Om-52 (Aqil), Om04-40 and -43 (Sayjah), Om04-12, -34 and -35 (Al Qurti). Related strong anomalies in multielement patterns and unusual ratios ($\text{Th/U} < 2.5$ and $\text{Th/Pb} > 5$) might indicate either post-magmatic alteration or open-system processes during magma ascent through the Arabian lithosphere.

4.3. Major elements and rock types

The analyzed lavas exhibit a wide range of SiO_2 (42 to 75 wt.%) and MgO contents (0.7 to 13 wt.%, Appendix B and Fig. 2a), even though mafic rocks ($\text{SiO}_2 < 53$ wt.% and $\text{MgO} > 3$ wt.%) are dominant. This chemical diversity is particularly obvious for the Umar samples which range from mafic to felsic (45-75 wt.% SiO_2 , 11.1-0.7 wt.% MgO, Appendix B). Among mafic lavas characterized by $\text{SiO}_2 < 53$ wt.% and a basaltic-type petrographic assemblage in thin section, samples with $\text{MgO} > 6$ wt.% were classified as basalts ($n = 26$) and samples with $3\% < \text{MgO} < 6$ wt.% as trachybasalts ($n = 16$). Both types have high P_2O_5 ($0.18 < \text{P}_2\text{O}_5 < 1.58$ wt.%) and high TiO_2 contents ($1.5 < \text{TiO}_2 < 3.6$ wt.%, Fig. 2b), with $\text{TiO}_2 < 2$ wt.% for only 7 out of 42 samples (Appendix B). These features are typical of alkaline magmas (Wilson, 1989). Despite the erratic behavior of alkali elements, a large majority of our sample set consistently plots within the alkaline field in the total alkali *versus* silica diagram (Fig. 2c). The very low $\text{Na}_2\text{O} + \text{K}_2\text{O}$ values of Umar Si-rich lavas (Om04-29, -34 and 35) are probably linked to the widespread alteration of their groundmass.

4.4. Trace elements

Most Hawasina Triassic basalts and trachybasalts show enrichment in LREE and depletion in HREE and Y, features that are characteristic of intraplate magmas (Sun and McDonough, 1989; Willbold and Stracke, 2006). Their multielement patterns are very similar to OIB patterns (Fig. 3a,b), with enrichments culminating at Nb (Appendix C). When plotted in the Zr/Ti *versus* Nb/Y and Nb/Y *versus* Zr/Y diagrams (Fig. 4a,b), most of the samples yield Nb/Y ratios higher than 1, consistent with an alkaline affinity (Winchester and Floyd, 1977). In Fig. 4b, the studied mafic lavas plot within the field of alkali basalts from the Icelandic Neo-Volcanic Zone and away from the fields of Icelandic tholeiites and N-MORB (Fitton et al., 1997; Kokfelt et al., 2006).

The multielement diagrams of the Umar samples cluster into two main geochemical groups. The first (and by far the largest) one displays high enrichments in the most incompatible elements together with fractionated patterns ($\text{La/Yb}_N > 15$, Fig. 3a) and Nb/Y ratios higher than 1. This population hereafter referred to as the “alkali group”, includes all the samples from the UmV₁ basal unit of the Umar Group (Al Qurti section) and most UmV₂ lavas. The second group exhibits less fractionated patterns, with a lesser enrichment in the most incompatible elements and a more subdued depletion in the least incompatible elements ($5 < \text{La/Yb}_N < 15$, Fig. 3a, Appendix C). It includes a few lavas (Om-29, Om04-40, Om04-51, Om-42 and -52 from UmV₂ unit of the Umar Group) that display Nb/Y ratios lower than 1, together with rather low Zr/Ti ratios (Fig. 4a). As these features are consistent with either a mildly alkaline or even sub-alkaline (Om04-40) affinity, this group will be referred to as the “sub-alkaline group”.

4.5. Nd and Pb isotopes

4.5.1. Nd isotopic data

The initial Nd isotopic ratios of 54 analyzed samples range from 0.51211 to 0.51261 (i.e. ϵNd_i from +5.32 to -4.45; Table 2). The 44 positive ϵNd_i values are distributed among all the studied units, whereas the 10 negative ϵNd_i values are associated to the alkaline lavas of the Al Qurti UmV₁ (5 samples) and Sinni (5 samples) sections of the Umar Group (Table 2). ϵNd_i values of the 31 Umar samples cluster into three main groups characterized by (i) unradiogenic ϵNd_i values ($-4.5 < \epsilon\text{Nd}_i < -1.2$), (ii) radiogenic ϵNd_i values ($2 < \epsilon\text{Nd}_i < 4.4$), and (iii) intermediate ϵNd_i values, including two samples (Om04-40 and Om-97) with ϵNd_i of 0.52 and 0.34, respectively. The ϵNd_i of the latter two Umar groups encompass those of Kawr flows and Al Aridh lavas ($0.7 < \epsilon\text{Nd}_i < 4.1$ and $1.2 < \epsilon\text{Nd}_i < 3.2$), while Kawr intrusions yield more radiogenic Nd isotopic ratios with $3.1 < \epsilon\text{Nd}_i < 5.3$ (Table 2).

4.5.2. Pb isotopic data

In Pb-Pb isotopic diagrams (Fig. 5a,b), Hawasina samples plot within an array subparallel to the Northern Hemisphere Reference Line (NHRL; Hart, 1984). Umar samples (n=23) exhibit highly variable Pb isotopic ratios, including both the most and the least radiogenic Pb compositions in our data set. They range from 16.35 to 19.31 for $(^{206}\text{Pb}/^{204}\text{Pb})_i$, from 15.28 to 15.64 for $(^{207}\text{Pb}/^{204}\text{Pb})_i$ and from 35.91 to 39.09 for $(^{208}\text{Pb}/^{204}\text{Pb})_i$ (Table 2). Kawr and Al Aridh samples plot between these extremes. Kawr intrusions exhibit a wide range of Pb ratios which straddle that of the Kawr flows and Al Aridh samples. In the Pb-Pb correlation diagrams, the five samples that show the highest deviations from the main trend in Th-U and Th-Pb diagrams (Appendix C) generally plot within the OIB field, with the exception of the Om04-34 rhyolite which yields very unusual Pb ratios (Table 2). Such initial recalculated ratios could be linked to an overcorrection due to its particularly high Th contents compared to its low Pb concentration (Appendix B). Thus, this sample will not be considered in the following discussion.

4.5.3. *Pb versus Nd isotopic ratios*

With the exception of Kawr intrusions, which exhibit highly variable Pb isotopic ratios together with a restricted range of ϵNd_i values, the studied sample set shows a rough positive correlation in the ϵNd_i versus $(^{206}\text{Pb}/^{204}\text{Pb})_i$ diagram (Fig. 5c). The observed scatter indicates that at least two isotopic end-members contributed to the geochemical signatures of the Hawasina Triassic magmatism (Fig. 5a,b,c).

5. Discussion

5.1. *Fractionation, assimilation coupled with fractional crystallization and partial melting effects*

The Umar UmV₂ trachyandesites, trachytes and rhyolites (Om04-17, -24, -27 and Om04-34 to -38) have negative Eu (and Ti) anomalies that are absent from UmV₁ and UmV₂ basaltic flows (Appendix C). The decrease of Al₂O₃ contents and Eu/Eu* ratios with increasing silica content (for SiO₂ > 53 wt.%, Fig. 6a,b) suggest that the Eu negative anomaly is correlated to plagioclase fractionation. However, a closed-system fractional crystallization process is not consistent with most REE variations. Indeed, UmV₂ basalts and trachyandesites (Om04-17 to 27) exhibit similar enrichments in La, but higher HREE and Y contents than UmV₁ basalts (Fig. 3a, Appendix C). Moreover, in Figure 6c, a jump in (La/Yb)_N ratios is observed between UmV₁ basalts and UmV₂ lavas. The whole sample set displays positive correlations between La and (La/Yb)_N (Fig. 6d), which are not consistent with closed-system fractionation.

The isotopic signatures of the studied lavas could be an intrinsic feature of their mantle source(s), or acquired *via* assimilation processes during magma ascent and/or storage within the Arabian lithosphere. Among our set, Umar samples exhibit the largest scatter of both SiO₂ contents and ϵNd_i values. Their SiO₂ contents and trace elements ratios were plotted against ϵNd_i values (Fig. 6e) to check the assimilation hypothesis. Umar alkali basalts seem to have preferentially sampled the Nd and Pb unradiogenic component. On the other hand, the silica-rich Umar lavas (UmV₂ trachyandesites, trachytes and rhyolites) exhibit ϵNd_i higher than those of basaltic lavas. Therefore, the relationships between the isotopic Nd signature and the silica contents of analyzed lavas are opposite to those expected for a shallow (upper) crustal assimilation process coupled with fractional crystallization (DePaolo, 1980), an increase of SiO₂ and a decrease in ϵNd_i .

The studied mafic lavas display (La/Yb)_N variations dependant from variable La contents (Fig. 6d) and from significant variations of the HREE (trend 1 in Fig. 7a). A sample subset shows, in contrast, significant evolution of Yb contents (Fig. 7c) and (Sm/Yb)_N ratios, without significant variations of La contents (trend 2 in Fig. 7a,b). As garnet has high distribution coefficients for HREE, (La/Yb)_N and (Sm/Yb)_N ratios are sensitive to the amount of residual garnet during partial melting (Caroff et al., 1997). An increasing melting degree of garnet-bearing lherzolite leads to a rapid decrease of La/Yb ratio without major Yb fractionation (Luhr et al., 1995). In contrast, increasing melting of spinel lherzolite will involve a more rapid Yb fractionation without significant variation of La/Yb ratio (Fig. 7c). In Figure 7c, Umar mafic lavas define two main trends delineated by the two grey domains. UmV₂ sub-alkaline basalts characterized by low (La/Yb)_N ratios (< 10) show significant (Sm/Yb)_N variations with highly variable Yb contents. They might derive from variable amounts of partial melting degrees (F ~ 5 to 10%) of a garnet-free lherzolithic source. In contrast, the older UmV₁ alkali basalts, which display high (La/Yb)_N ratios (> 15) and low Yb contents (< 2 ppm) might derive from a lower amount (F ~ 3 to 6 %) of partial melting of a deeper (garnet+spinel-bearing) lherzolithic source. The Kawr and Al Aridh mafic lavas plot between the two Umar groups (Fig. 7c) and could have been generated at intermediate depths.

5.2. Evidence for source heterogeneity

The investigated mafic lavas display geochemical features similar to OIB and continental intraplate basalts, i.e. (i) incompatible element enrichments (Fig. 3) and (ii) Nd and Pb isotopic compositions clearly distinct from MORB (Fig. 5c). The most Nd- and Pb-radiogenic samples plot within the OIB field (Fig. 5), while the least Nd- and Pb-radiogenic ones (Umar alkali basalts) plot close to the Enriched Mantle 1 end-member (EM 1, Zindler and Hart, 1986; Fig. 5c). Their principal mantle source is distinct from the Depleted MORB Mantle

(DMM) in that the highest ϵNd_i value is +5.3 (Table 2). Moreover, the isotopic signatures of the Umar alkali basalts suggest a contribution of another source, one characterized by strongly enriched LREE patterns (Fig. 3a) relatively high La/Nb and Th/Nb ratios (Fig. 8a,b) and negative ϵNd_i signatures ($-4.5 < \epsilon\text{Nd}_i < -1.2$) (Figs. 5c and 8).

In addition, the $(\text{La}/\text{Sm})_N$ versus ϵNd_i plot (Fig. 8c) shows that the LREE enrichment of the basaltic samples is not coupled with Nd isotopic ratios. Indeed, it is greatest in the low ϵNd_i group (Umar basalts) and in the high ϵNd_i Kawr platform intrusions. In this diagram, the occurrence of two distinct isotopic groups and the lack of continuous trends suggest that the studied samples do not derive from the melting of variable mixes of two main mantle components. In that respect, they differ from most hotspot lavas which usually plot along linear trends connecting a depleted and an enriched mantle component in diagrams of Nd and Pb isotopic ratios and incompatible trace elements (Phipps Morgan and Morgan, 1999).

5.3. Possible geochemical imprint of the Arabian lithosphere

In the Ti/Y versus ϵNd_i plot (Fig. 8d), the studied basalts and trachybasalts show geochemical signatures characteristic of high-Ti continental flood basalts ($\text{Ti}/\text{Y} > 300$ -350; Hawkesworth et al., 1992; Gibson et al., 1995; Peate and Hawkesworth, 1996; Pik et al., 1998, 1999). Highly variable ϵNd_i values such as those observed for Hawasina lavas are often a characteristic of continental basalts. They are generally interpreted as markers of interactions between asthenosphere-derived melts and the local continental crust or the subcontinental lithospheric mantle (Saunders et al., 1992; Lightfoot et al., 1993; Sharma, 1997). As shown in Figs. 8a-b, the low ϵNd_i lavas from the Umar display a slight but significant depletion in Nb. This feature might be attributed to interactions with the local continental lithosphere, e.g. the lower crust or subcontinental lithospheric mantle.

The Arabo-Nubian shield includes oceanic terranes that formed and accreted during the Neoproterozoic Pan-African orogeny (Stern, 1994; Stein and Goldstein, 1996). These terranes are characterized by radiogenic Nd and Pb isotopic ratios ($+2 < \epsilon\text{Nd}_i < +9$; Stoesser and Frost, 2006; Andersson et al., 2006). In addition, mafic and felsic granulites and peridotites, locally exhumed or found as xenoliths within Cenozoic lavas, sample of the Arabo-African lower continental crust and lithospheric mantle (Fig. 9). Their isotopic characteristics define a large domain of variation with, for instance, radiogenic Pb compositions ($^{206}\text{Pb}/^{204}\text{Pb} > 18$) and positive ϵNd_i signatures for Zabargad granulites and peridotites (Lancelot and Bosch, 1991; Hamelin and Allègre, 1988). Moreover, xenoliths from the Arabo-African lithospheric mantle also display radiogenic Nd ratios ($0.5135 < ^{143}\text{Nd}/^{144}\text{Nd} < 0.5129$), associated to $^{206}\text{Pb}/^{204}\text{Pb} > 17$: these values are intermediate between DMM and high- μ (HIMU) end-members (Fig. 9). In addition, the predominant HIMU isotopic signature ($^{206}\text{Pb}/^{204}\text{Pb} = 18.60$ to 19.55) of

Neogene-Quaternary intraplate basalts in Syria, Saudi Arabia and Yemen, has been interpreted as inherited from the Arabian lithospheric mantle (Bertrand et al., 2003).

The positive ϵNd of the Arabian lithospheric mantle (Fig. 9b) precludes it as the main source of the studied lavas, which have negative ϵNd values. Conversely, both the Nd and Pb isotopic ratios of the studied lavas plot within the compositional range of the Arabian upper and lower crusts. In particular, the isotopic compositions of alkali UmV₁ basalts match those of mafic granulites from the Yemen lower crust (Baker et al., 1997). This feature together with their slight Nb depletion suggests that the UmV₁ lavas signature might result from assimilation of lower crustal materials (Fig. 8a,b).

5.4. A Triassic Neotethyan plume beneath the Oman margin?

The OIB-like characteristics and predominantly alkali basaltic features of the Triassic Hawasina lavas have led many former authors (Glennie et al., 1974; Searle et al., 1980; Searle and Graham, 1982; Robertson and Searle, 1990; Stampfli et al., 1991; Pillevuit, 1993; Pillevuit et al., 1997) to consider them as hotspot-related intra-oceanic plateaus or seamounts. They might derive from either a genuine Triassic mantle plume or a still active Tethyan plume inherited from the Permian magmatic history. However, any isotopic (Figs. 5c and 10) or trace element (Fig. 4b) evidence for a depleted mantle component in their source is lacking. Conversely, Triassic depleted tholeiites occur in the Mamonia Complex, Cyprus (Lapierre et al., 2007), in Baër Bassit, Syria (Perez, 2006) and in Othrys, Greece (Monjoie et al., 2008). The isotopic signatures of Mediterranean Triassic volcanics (Fig. 10) are consistent with a mixing between the depleted upper mantle (main source of Mamonia, Baër Bassit and Othrys depleted tholeiites) and two mantle enriched components, HIMU and EM 2 (Perez, 2006; Lapierre et al., 2007; Maury et al., 2008). In contrast with the Oman case, none of these volcanics involved the contribution of lower crustal components with negative ϵNd_i to their genesis (Fig. 10). This feature suggests that they were emplaced on the Neotethyan oceanic floor rather than on a continental margin.

In addition, the hypothesis of a Triassic plume beneath the Oman margin does not fit available geological and chronological constraints. The preserved Triassic lava piles are less than 100 m thick, and thus very small with respect to plume-related magmatic successions such as traps, oceanic islands or rift-related series. The comparison of the Kawr platform with an intra-oceanic atoll built on the top of a seamount (Pillevuit, 1993; Pillevuit et al., 1997) has been invalidated by recent fieldwork (Basile and Chauvet, 2009). In addition, there is no evidence for magmatic activity in the Oman margin between the Permian (Wordian-Capitanian, ca. 265 Ma old) and the Middle-Late Triassic (Ladinian-Carnian, ca. 230 Ma old)

events. This time gap is inconsistent with the hypothesis of survival of a Neotethyan plume since the Permian event.

5.5. An alternative hypothesis: melting of the Oman lithospheric mantle modified by the Permian plume.

Alkali basaltic magmas can be emplaced in regions removed from a mantle plume, providing that a distensional tectonic regime causes the uprise and partial melting of enriched lithospheric mantle (Wilson, 1989). Passage over an active mantle plume can indeed modify considerably the composition of the oceanic (Dupuy et al., 1993; Chauvel et al., 1997) or continental (Hawkesworth et al., 1990; Saunders et al., 1992; Lightfoot et al., 1993) lithospheric mantle, mainly through melt-induced metasomatism (Harry and Leeman, 1995; Downes, 2001). For instance, enriched pargasite-bearing mantle xenoliths from Morocco record the pervasive metasomatism of a depleted Proterozoic sublithospheric mantle by Tertiary plume-related HIMU-type alkaline melts which obliterated its initial composition (Raffone et al., 2009). The HIMU signature of Cenozoic alkali basalts from western Europe and their mantle xenoliths is attributed to mantle metasomatism of an heterogeneous lithospheric mantle by melts from an Early Tertiary asthenospheric plume (Hoernle et al., 1995; Downes, 2001). To test such a process, we have compared the compositions of the studied Triassic Hawasina lavas and those of their predecessors, i.e. the Permian Hawasina basalts which are clearly plume-related (Maury et al., 2003; Lapierre et al., 2004).

The Permian Hawasina basaltic piles include high-Ti alkali melts and low-Ti tholeiitic melts (Fig. 11a), the latter displaying low $(La/Sm)_N$ ratios (Fig. 11b) and either slightly enriched or slightly depleted multielement patterns (Fig. 11c). On the basis of Nd and Pb isotopic data, Lapierre et al. (2004) defined three different geochemical groups. Group 1 low-Ti tholeiitic basalts are characteristic of the most distal environments of the Hawasina Permian basin. They have variable but radiogenic Nd isotopic ratios ($3.8 < \epsilon Ndi < 11.1$, Fig. 12a,b), together with rather homogeneous Pb isotopic ratios (Fig. 12c). Group 2 high-Ti alkali basalts are systematically associated with the proximal basin environments, and are more enriched in La, Th and Nb than Group 1 basalts (Fig. 11b,c). They are characterized by less radiogenic Nd isotopic ratios ($3.1 < \epsilon Ndi < 4.9$; Fig. 12a,b). Finally, Group 3 includes high-Ti and low-Ti basalts (Fig. 11a) that erupted onto the continental platform of the Arabian margin, except for one basalt from the distal basin (top left of Fig. 11c). These Group 3 basalts are systematically enriched in the most incompatible trace elements and they have unradiogenic Nd isotopic ratios ($-2 < \epsilon Ndi < 1.6$) and Pb isotopic ratios similar to those of Group 2 lavas (Fig. 12).

The trace element compositions of the Triassic Hawasina volcanics are overall very similar to those of Groups 2 and 3 high-Ti Permian basalts (Fig. 11c). Moreover, with the exception of Kawr intrusions and UmV₁ alkali basalts, the Nd and Pb isotopic compositions of Triassic Hawasina basalts match those of Groups 2 and 3 Permian basalts (Fig. 12). The UmV₁ basalts show Nd and Pb compositions less radiogenic than those of Group 3 lavas (Fig. 12c).

The above comparison shows that a component equivalent to that which generated the Permian Group 1 distal tholeiites has not been detected in the studied samples. Conversely, the Hawasina Triassic lavas are isotopically similar to Permian Groups 2 and 3 lavas, respectively (Fig. 12c). It is therefore possible to consider the OIB-type source of Permian Group 2 alkali basalts as identical or closely similar to the source of most Triassic volcanics (UmV₂ unit, Kawr intrusions and the majority of Al Aridh lavas). It might thus represent the main mantle reservoir underlying the Arabian margin since Middle Permian times (component A in Fig. 12a,b). The Kawr intrusions, which display higher La/Sm and La/Nd ratios than other Triassic lavas, could derive from low-degree melting of this source (trend B in Fig. 12a,b).

In the La/Nb, (La/Sm)_N and La/Nd *versus* εNdi diagrams (Figs. 8a and 12a,b), Kawr basaltic flows plot between the main radiogenic and unradiogenic components. Trend C, drawn in (La/Sm)_N and La/Nd *versus* εNdi plots, suggests that their source might be a mixture between OIB-type mantle (component A) and an enriched component. This trend has no equivalent among the Permian basalts, but the number of samples defining it is too limited for detailed interpretation.

Finally, the trend towards EM 1 (Fig. 12c) of Permian Group 3 and Triassic UmV₁ alkali basalts might result from their interaction with the lower crust (trend D in Fig. 12a,b). According to Lapierre et al. (2004), contamination of Group 3 Permian lavas would involve rocks similar in composition to the gneissic granulites of Zabargad Island. In contrast, UmV₁ basalts have Nd and Pb isotopic ratios that are lower than those of Zabargad granulites (Fig. 9), and more consistent with the composition of mafic lower crustal xenoliths (Baker et al., 1997).

In short, we propose that Permian plume-related alkaline melts metasomatized the Oman lithospheric mantle during their ascent towards the surface, overprinting its initial DMM-HIMU signature. Thirty-five million years later, a post-breakup extension induced partial melting of this metasomatized mantle, and generated the Triassic basaltic magmas. During their ascent, some of the oldest and deepest melts (UmV₁ basalts) interacted with rocks from the lower continental crust.

5.6. Tectonic framework of the Triassic volcanic event

Coeval (Ladinian – Carnian) volcanic sequences were emplaced all along the southern Tethyan realm. They were interpreted either as belonging to the southern Neotethyan continental margin series (e.g. Béchevrec et al., 1988, 1991) or alternatively as oceanic island on the Neotethyan oceanic floor (Stampfli et al. 1991; Pillevuit et al., 1997). The lower crustal contamination suffered by the oldest Triassic basalts in the Umar basin (UmV₁) indicates that distal parts of the Hawasina basin overlay continental crust during the Triassic. The concomitant synsedimentary destabilizations of its continental slope and basin environments (Watts, 1990; Pillevuit, 1993) suggest a link between the Triassic magmatic event and extensional (post-breakup) tectonic reactivation of the Permian structures.

The Neotethys opened between the northern edge of Gondwana and the Cimmerian continental blocks. These blocks drifted northward during the subduction of the Paleotethys beneath the Southern Laurasia active margin (Besse et al., 1998). At the end of the Middle Triassic (Anisian), Paleotethyan subduction ended and was replaced by that of the Neotethys (Saidi et al., 1997; Besse et al., 1998). In geodynamic reconstructions, this subduction jump is generally linked to a global kinematic reorganization of the Tethyan realm. It is either attributed to a Neotethys ridge jump (Dercourt et al., 1993; Besse et al., 1998; Vrielynck and Bouysse, 2001), or to a change from a transtensional to a distensional regime in the Neotethys accretion system (Ricou, 1994). Both processes might lead to a reactivation of the extensional tectonic structures inherited from the Permian breakup. The resulting extension might have caused convective thinning of the subcontinental lithosphere similarly to that in the Basin and Range province (Fitton et al., 1991; DePaolo and Daley, 2000). We suggest that this thinning led to the decompression-triggered partial melting of the Arabian uprising mantle, and to the emplacement of the Triassic Hawasina basalts.

6. Conclusions

1. Middle to Late Triassic volcanic rocks from the Hawasina Nappes are predominantly alkali basalts, with minor associated sub-alkaline basalts, trachyandesites, trachytes and rhyolites. Most of them are geochemically very similar to the more abundant Permian plume-related high-Ti basalts, which also occur in the Hawasina Nappes.

2. The Triassic basalts derive from low-degree melting of an enriched OIB-type mantle source, characterized by $0.3 < \epsilon Nd_i < 5.3$ and $^{206}Pb/^{204}Pb_i = 16.96-19.31$. With time, the degree of partial melting increased and the corresponding depths decreased from the garnet + spinel to the spinel lherzolite facies. Some of the oldest and deepest melts (UmV₁ unit of Umar Group) are distinguished from the others by their unradiogenic Nd and Pb signature, with -

4.5 < ϵNd_i < -1.2 and $^{206}\text{Pb}/^{204}\text{Pb}_i = 16.35\text{-}17.08$. We attribute these features to contamination by the lower continental crust of the Oman margin.

3. The Triassic Hawasina lavas show no evidence for a depleted mantle source, such as those documented for the Permian tholeiitic low-Ti basalts of Oman and the Triassic oceanic island-type tholeiites of Cyprus. The ca. 35 My time span between their emplacement and that of their Permian equivalents suggests that they were not related to prolonged activity of the Tethyan plume. We propose instead that they originated from the partial melting of the Oman lithospheric mantle, the original DM-HIMU signature of which was overprinted during its pervasive metasomatism by Permian plume-related melts.

4. The origin of the Hawasina Triassic volcanism is tentatively attributed to a post-breakup decompression-triggered melting event linked to an extensional remobilization of the earlier tectonic structures of the Oman margin. This remobilization was possibly a consequence of the global kinematic reorganization of the Tethyan realm during the Middle Triassic.

Acknowledgements

This study was initiated by the late Professor Jean Marcoux, Université de Paris 7, who communicated to us his enthusiasm for the study of the Tethyan margin in Oman. It was funded by the Institut National des Sciences de la Terre, programme “Intérieur de la Terre”, the Groupement de Recherche “Marges”, CNRS UMR 5025 (Université Joseph Fourier, Grenoble) and UMR 6538 (Université de Bretagne Occidentale, Brest), and the BRGM Research Division. Critical comments by Drs. Sobhi Nasir, Michel Grégoire and an anonymous reviewer, together with editorial comments by Dr. Andrew Kerr, led to considerable shortening and improvement of the initial manuscript. We also thank Nick Arndt for checking the revised version. We acknowledge the authority of Oman and especially thank Dr. Hilal Mohammed Sultan Al Azry, Director of the Geological Survey, Omani Ministry of Commerce and Industry, for his welcome and support in Oman. Dr. François Béchenec is thanked for his contribution to field studies, stimulating discussions and useful comments on the manuscript.

References

Ahmad, T., Islam R., Khanna, P.P., Thakur, V.C., 1996. Geochemistry, petrogenesis and tectonic significance of the basic volcanic units of the Zildat ophiolitic mélange, Indus suture zone, eastern Ladakh (India). *Geodinamica Acta* 9, 222-233.

574

575 Al Riyami, K., Robertson, A.H.F., 2002. Mesozoic sedimentary and magmatic evolution
576 of the Arabian continental margin, northern Syria: evidence from the Baer-Bassit Melange.
577 Geological Magazine 139, 395-420.

578

579 Altherr, R., Henjes-Kunst, F., Baumann, A., 1990. Asthenosphere versus lithosphere as
580 possible sources for basaltic magmas erupted during formation of the Red Sea: constraints
581 from Sr, Pb and Nd isotopes. Earth and Planetary Science Letters 96, 269-286.

582

583 Andersson, U.B., Ghebreab, W., Teklay, M., 2006. Crustal evolution and metamorphism
584 in east-Eritrea south-east Arabian-Nubian Shield. Journal of African Earth Sciences 44, 45-
585 65.

586

587 Baker, J. A., Menzies, M.A., Thirlwall, M.F., Macpherson, C.G., 1997. Petrogenesis of
588 Quaternary intraplate volcanism, Sana'a, Yemen: implications for plume lithosphere
589 interaction and polybaric melt hybridization. Journal of Petrology 38, 1359-1390.

590

591 Baker, J.A., Macpherson, C.G., Menzies, M.A., Thirlwall, M.F., Al-Kadasi, M., Matthey,
592 D.P., 2000. Resolving crustal and mantle contributions to continental flood volcanism,
593 Yemen: Constraints from mineral oxygen isotope data. Journal of Petrology 41, 1805-1820.

594

595 Baker, J.A., Chazot, G., Menzies, M A., Thirlwall, M., 2002. Lithospheric mantle beneath
596 Arabia: A Pan-African protolith modified by the Afar and older plumes, rather than a source
597 for continental volcanism? In: Menzies, M.A., Klemperer, S.L., Ebinger, C.J., Baker, J.
598 (Eds.), Volcanic Rifted Margins. Geological Society of America Special Paper, vol. 362, pp.
599 65-80.

600

601 Barrat, J.A., Keller, F., Amossé, J., 1996. Determination of rare earth elements in sixteen
602 silicate reference samples by ICP-MS after Tm addition and ion exchange separation.
603 Geostandard Newsletter 20, 133-139.

604

605 Basile, C., Chauvet, F., 2009. Hydromagmatic eruption during the buildup of a Triassic
606 carbonate platform (Oman Exotics): eruptive style and associated deformations. Journal of
607 Volcanology and Geothermal Research 183, 84-96.

608

Baud, A., Béchenec, F., Cordey, F., Krystyn, L., Le Métour, J., Marcoux, J., Maury, R.,
Richoz, S., 2001. Permo-Triassic deposits: from the platform to the basin and seamounts.
International Conference on the Geology of Oman, Excursion, n°A01, 56 p.

Béchenec, F., 1987. Géologie des Nappes Hawasina dans les parties orientale et centrale
des Montagnes d'Oman. Thèse Doctorat d'Etat, Université Pierre et Marie Curie, Paris VI,
Document du BRGM 127, 474 p.

Béchenec, F., Le Métour, J., Platel, J.P., Roger, J., 1993. Geological map of the Sultanate
of Oman, scale 1/1000000, Explanatory notes; Sultanat of Oman. Ministry of Petroleum and
Minerals, Directorate General of Minerals (Ed.).

Béchenec, F., Le Métour, J., Rabu, D., Villet, M., Beurrier, M., 1988. The Hawasina
Basin: a fragment of a starved passive continental margin, thrust over the Arabian Platform
during obduction of the Sumail Nappe. *Tectonophysics* 151, 323-343.

Béchenec, F., Le Métour, J., Rabu, D., Bourdillon-Jeudy de Grissac, C., De Wever, P.,
Beurrier, M., Villet, M., 1990. The Hawasina Nappes: stratigraphy, paleogeography and
structural evolution of a fragment of the south-Tethyan passive continental margin. In:
Robertson, A.H.F., Searle, M.P., Ries, A.C. (Eds.), *The Geology and Tectonics of the Oman
Region*. Geological Society Special Publication 49, pp. 213-223.

Béchenec, F., Tegye, M., Le Métour, J., Lemièr, B., Lescuyer, J.L., Rabu, D., Milési,
J.P., 1991. Igneous rocks in the Hawasina nappes and the Al-Hajar supergroup, Oman
mountains: their significance in the birth and evolution of the composite extensional margin
of eastern Tethys. In: Peters, T., Nicolas, A., Coleman, R.G. (Eds.), *Ophiolite genesis and
evolution of the oceanic lithosphere*. Ministry of Petroleum and Minerals, Directorate General
of Minerals of Oman, Kluwer, pp. 569-611.

Bertrand, H., Chazot, G., Blichert-Toft, J., Thorval, S., 2003. Implications of widespread
high- μ volcanism on the Arabian Plate for Afar mantle plume and lithosphere composition.
Chemical Geology 198, 47-61.

Bernouilli, D., Weissert, H., 1987. The upper Hawasina nappes in the central Oman
mountains: stratigraphy, palinspatics and sequence of nappes emplacement. *Geodinamica
Acta* 1, 47-58.

645

646 Besse, J., Torcq, F., Gallet, Y., Ricou, L.E., Krystyn, L., Saidi, A., 1998. Late Permian to
647 Late Triassic paleomagnetic data from Iran: constraints on the migration of the Iranian block
648 through the Tethyan Ocean and initial destruction of Pangaea. *Geophysical Journal*
649 *International* 135, 77-92.

650

651 Beurrier, M., Béchenec, F., Rabu, D., Hutin, G., 1986. Geological map of Rustaq: Sheet
652 NF40-3A, Scale 1/100 000, Sultanate of Oman. Ministry of Petroleum and Minerals,
653 Directorate General of Minerals (Ed.).

654

655 Blusztajn, J., Hart, S.R., Shimizu, N., McGuire, A.V., 1995. Trace element and isotopic
656 characteristics of spinel peridotite xenoliths from Saudi Arabia. *Chemical Geology* 123, 53-
657 65.

658

659 Bosch, D., Blichert-Toft J., Moynier, F., Nelson, B.K., Telouk, P., Gillot, P.Y., Albarède,
660 F., 2008. Pb, Hf and Nd isotope compositions of the two Réunion volcanoes, Indian Ocean: a
661 tale of two small-scale mantle “blobs”. *Earth and Planetary Science Letters* 265, 748-768.

662

663 Caroff, M., Maury, R.C., Guille, G., Cotten, J., 1997. Partial melting below Tubuai
664 (Austral Islands, French Polynesia). *Contributions to Mineralogy and Petrology* 127, 369–
665 382.

666

667 Chan, G.H.-N., Malpas, J., Xenophontos, C., Lo, C.-H., 2008. Magmatism associated with
668 Gondwanaland rifting and Neo-Tethyan oceanic basin development: evidence from the
669 Mamonia Complex, SW Cyprus. *Journal of the Geological Society London* 165, 699-709.

670

671 Chauvel, C., McDonough, W., Guille, G., Maury, R.C., Duncan, R., 1997. Contrasting old
672 and young volcanism in Rurutu Island, Austral chain. *Chemical Geology* 139, 125-143.

673

674 Chauvel, C., Blichert-Toft, J., 2001. A hafnium isotope and trace element perspective on
675 melting of the depleted mantle. *Earth and Planetary Science Letters* 190, 137-151.

676

677 Chauvet, F., Lapierre, H., Bosch, D., Guillot, S., Mascle, G., Vannay, J.-C., Cotten, J.,
678 Brunet, P., Keller, F., 2008. Geochemistry of the Panjal Traps basalts (NW Himalaya):
679 records of the Pangea Permian break-up. *Bulletin de la Société Géologique de France* 179,
680 383 - 395.

681

682 Cohen, R.S., O'Nions, R.K., Dawson, J.B., 1984. Isotope geochemistry of xenoliths from
683 East Africa: implications for development of mantle reservoirs and their interaction. *Earth*
684 *Planetary Science Letters* 68, 209-220.

685

686 Coleman, R.G., 1981. Tectonic setting for ophiolite obduction in Oman. *Journal of*
687 *Geophysical Research* 86, 2497-2508.

688

689 Corfield, R.I., Searle, M.P., Green, O.R., 1999. Photang thrust sheet: an accretionary
690 complex structurally below the Spongtag ophiolite constraining timing and tectonic
691 environment of ophiolite obduction, Ladakh Himalaya, NW India. *Journal of the Geological*
692 *Society London* 156, 1031-1044.

693

694 Cotten, J., Le Dez, A., Bau, M., Caroff, M., Maury, R.C., Dulski, P., Fourcade, S., Bohn,
695 M., Brousse, R., 1995. Origin of anomalous rare-earth element and yttrium enrichments in
696 subaerially exposed basalts: evidence from French Polynesia. *Chemical Geology* 119, 115-
697 138.

698

699 Davidson, J. P., Wilson, I. R., 1989. Evolution of an alkali basalt-trachyte suite from Jebel
700 Marra volcano, Sudan, through assimilation and fractional crystallization. *Earth and Planetary*
701 *Science Letters* 95, 141-160.

702

703 DePaolo, D.J., 1980. Trace element and isotopic effects of combined wallrock
704 assimilation and fractional crystallization, *Earth and Planetary Science Letters* 53, 189-202.

705

706 DePaolo, D.J., Daley, E.E., 2000. Neodymium isotopes in basalts of the southwest basin
707 and range and lithospheric thinning during continental extension. *Chemical Geology* 169,
708 157-185.

709

710 Dercourt, J., Ricou, L.E., Vrielynck, B. (Eds.), 1993. *Atlas Tethys Palaeoenvironmental*
711 *Maps*. Gauthier-Villars, Paris, 14 maps.

712

713 De Wever, P., Bourdillon de Grissac, C., Bechennec F., 1990. Permian to Cretaceous
714 radiolarian biostratigraphic data from the Hawasina Complex, Oman Mountains. In:
715 Robertson, A.H.F., Searle, M.P., Ries, A.C. (Eds.), *The Geology and Tectonics of the Oman*
716 *Region*. Geological Society Special Publication 49, pp. 225-238.

Downes, H., 2001. Formation and modification of the shallow sub-continental lithospheric mantle: a review of geochemical evidence from ultramafic xenolith suites and tectonically emplaced ultramafic massifs of western and central Europe. *Journal of Petrology* 42, 233-250.

Dupuy, C., Vidal, P., Maury, R.C., Guille, G., 1993. Basalts from Mururoa, Fangataufa and Gambier islands (French Polynesia): geochemical dependance on the age of the lithosphere. *Earth Planetary Science Letters* 117, 89-100.

Fitton, J.G., James, D., Leeman, W.P., 1991. Basic magmatism associated with Late Cenozoic extension in the western United States: compositional variations in space and time. *Journal of Geophysical Research* 96 (B8), 13,693-13,711.

Fitton, J.G., Saunders, A.D., Norry, M.J., Hardarson, B.S., Taylor, R.N., 1997. Thermal and chemical structure of the Iceland plume. *Earth and Planetary Science Letters* 153, 197-208.

Garzanti, E., Le Fort, P., Sciunnach, D., 1999. First report of Lower Permian basalts in South Tibet: tholeiitic magmatism during break-up and incipient opening of Neotethys. *Journal of Asian Earth Sciences* 17, 533-546.

Gibson, S.A., Thompson, R.N., Dickin, A.P., Leonardos, O.H., 1995. High-Ti and low-Ti mafic potassic magmas: Key to plume-lithosphere interactions and continental flood-basalt genesis. *Earth and Planetary Science Letters* 136, 149-165.

Glennie, K.W., Bœuf, M.G.A., Hughes Clarke, M.W., Moody-Stuart, M., Pilaart, W.F.H., Reinhardt, B.M., 1974. *Geology of the Oman mountains*. *Geologie en Mijnbouw*, 1, 423 p.

Hamelin, B., Allègre, C. J., 1988. Lead isotope study of orogenic lherzolite massifs. *Earth and Planetary Science Letters* 91, 117-131.

Harry, D.L., Leeman, W.P., 1995. Partial melting of melt metasomatized subcontinental mantle and the magma source potential of the lower lithosphere. *Journal of Geophysical Research* 100 (B7), 10,255-10,269.

- Hart, S. R., 1984. A large isotope anomaly in the Southern Hemisphere mantle. *Nature* 309, 753-757.
- Hawkesworth, C. J., Kempton, P. D., Rogers, N. W., Ellam, R. M., van Calsteren, P. W., 1990. Continental mantle lithosphere, and shallow level enrichment processes in the Earth's mantle. *Earth and Planetary Science Letters* 96, 256-268.
- Hawkesworth, C.J., Gallagher, K., Kelley, S., Mantovani, M., Peate, D.W., Regelous, M., Rogers, N.W., 1992. Paraná magmatism and opening of the South Atlantic. In: Storey, B.C. Alabaster, T., Pankhurst, R.J. (Eds.), *Magmatism and the causes of continental break up*. Geological Society Special Publication 68, pp. 221-240.
- Hegner, E., Pallister, J.S., 1989. Pb, Sr, and Nd isotopic characteristics of Tertiary Red Sea rift volcanics from the central Saudi Arabian coastal plain. *Journal of Geophysical Research*, 94, 7749-7755.
- Hoernle, K., Zhang, Y.S., Graham, D., 1995. Seismic and geochemical evidence for large-scale mantle upwelling beneath the eastern Atlantic and western and central Europe. *Nature* 374, 34-39.
- Kokfelt, T.F., Hoernle, K., Hauff, F., Fiebig, J., Werner, R., Garbe-Schönberg, D., 2006. Combined trace element and Pb-Nd-Sr-O isotope evidence for recycled oceanic crust (upper and lower) in the Iceland mantle plume. *Journal of Petrology* 47, 1705-1749.
- Lancelot, J.R., Bosch, D., 1991. A Pan-African age for the HP-HT granulite gneisses of Zabargad island: implications for the early stages of the Red Sea rifting. *Earth and Planetary Science Letters* 107, 539-549.
- Lapierre, H., Bosch, D., Narros, A., Mascle, G. H., Tardy, M., Demant A., 2007. The Mamonia Complex (SW Cyprus) revisited: remnant of Late Triassic intra-oceanic volcanism along the Tethyan southwestern passive margin. *Geological Magazine* 144, 1-19.
- Lapierre, H., Dupuis, V., Mercier De Lepinay, B., Tardy, M., Ruiz, J., Maury, R.C., Hernandez, J., Loubet, M., 1997. Is the lower Duarte igneous complex (Hispaniola) a remnant of the Caribbean plume-generated oceanic plateau ? *Journal of Geology* 105(1), 111-120.

787

788 Lapierre, H., Samper, A., Bosch, D., Maury, R.C., Bechennec, F., Cotten, J., Demant, A.,
789 Brunet, P., Keller, F., Marcoux, J., 2004. The Tethyan plume: geochemical diversity of
790 Middle Permian basalts from the Oman rifted margin. *Lithos* 74, 167-198.

791

792 Le Bas, M.J., Le Maitre, R.W., Streickheisen, A., Zanettin, B., 1986. A chemical
793 classification of igneous rocks based on the total-alkali-silica diagram. *Journal of Petrology*
794 27, 745-750.

795

796 Lightfoot, P.C., Hawkesworth, C.J., Hergt, J., Naldrett, A.J., Gorbachev, N.S.,
797 Fedorenko, V.A., Doherty, W. 1993. Remobilisation of the continental lithosphere by a
798 mantle plume: major- trace- element, and Sr- Nd- and Pb-isotope evidence from picritic and
799 tholeiitic lavas of the Noril'sk District, Siberian Traps, Russia. *Contributions to Mineralogy*
800 and *Petrology* 114, 171-188.

801

802 Lippard, S.J., Shelton, A.W., Gass, I.G., 1986. The Ophiolite of northern Oman.
803 Geological Society of London, Memoir 11, 178 pp.

804

805 Luhr, J.F., Aranda-Gómez, J.J., Housh, T.B., 1995. San Quintín Volcanic Field, Baja
806 California Norte, México. Geology, petrology and geochemistry. *Journal of Geophysical*
807 *Research* 100 (B7), 10353–10380.

808

809 MacDonald, G. A., Katsura, T., 1964. Chemical composition of Hawaiian lavas. *Journal*
810 *of Petrology* 5, 82-133.

811

812 Maury, R.C., Béchennec, F., Cotten, J., Caroff, M., Cordey, F., Marcoux, J., 2003. Middle
813 Permian plume-related magmatism of the Hawasina Nappes and the Arabian Platform:
814 implications on the evolution of the Neotethyan margin in Oman. *Tectonics* 22 (6), 1073,
815 doi:10.129/2002TC001483.

816

817 Maury, R.C., Lapierre, H., Bosch, D., Marcoux, J., Krystyn, L., Cotten, J., Bussy, F.,
818 Brunet, P., Sénebier, F., 2008. The alkaline intraplate volcanism of the Antalya Nappes
819 (Turkey): a Late Triassic remnant of the Neotethys. *Bulletin de la Société géologique de*
820 *France* 179, 397-410.

821

- McDonough, W.F., 1990. Constraints on the composition of the continental lithospheric mantle. *Earth and Planetary Science Letters* 101, 1-18.
- McLennan, S., 2001. Relationships between the trace element composition of sedimentary rocks and upper continental crust. *Geochemistry Geophysics Geosystems* 2, paper number 2000GC000109.
- Monjoie, P., Lapierre, H., Tashko, A., Mascle, G.H., Dechamp, A., Muceku, B., Brunet, P., 2008. Nature and origin of the Triassic volcanism in Albania and Othrys: a key to understanding the NeoTethys opening? *Bulletin de la Société géologique de France* 179, 411-425.
- Peate, D.W., Hawkesworth, C.J., 1996. Lithospheric to Asthenospheric transition in Low-Ti flood basalts from southern Parana, Brazil, *Chemical Geology* 127, 1-24.
- Perez, C., 2006. Le magmatisme de la marge arabique au Trias et Jurassique: analyses pétrogéochimiques dans la région du Baër-Bassit (Syrie) et implications géodynamiques. *Mem. M2R, Univ. J. Fourier, Grenoble*, 46 p.
- Phipps Morgan, J., Morgan, W.J., 1999. Two-stage melting and the geochemical evolution of the mantle: a recipe for mantle plum-pudding. *Earth and Planetary Science Letters* 170, 215-239.
- Pik, R., Deniel, C., Coulon, C., Yirgu, G., Hofmann, C., Ayalew, D., 1998. The Northwestern Ethiopian plateau flood basalts: Classification and spatial distribution of magma types. *Journal of Volcanology Geothermal Research* 81, 91–111.
- Pik, R., Deniel, C., Coulon, C., Yirgu, G., Marty, B., 1999. Isotopic and trace element signatures of Ethiopian flood basalts: Evidence for plume–lithosphere interactions. *Geochimica Cosmochimica Acta* 63(15), 2263–2279.
- Pillevuitt, A., 1993. Les Blocs Exotiques du Sultanat d'Oman, *Mémoires de Géologie, Lausanne* vol. 17, 249 p.
- Pillevuitt, A., Marcoux, J., Stampfli, G., Baud, A., 1997. The Oman Exotics: a key for the understanding of the Neotethyan geodynamic evolution. *Geodinamica Acta* 10 (5), 209-238.

858

859 Raffone, N., Chazot, G., Pin, C., Vanucci, R., Zanetti, A., 2009. Metasomatism in the
860 lithospheric mantle beneath Middle Atlas (Morocco) and the origin of Fe- and Mg-rich
861 wehrlites. *Journal of Petrology* 50, 197-249.

862

863 Ricou, L.E., 1994. Tethys reconstructed: plates, continental fragments and their
864 boundaries since 260 My from Central America to South-Eastern Asia. *Geodinamica Acta* 7,
865 169-218.

866

867 Robertson, A.H.F., Searle, M.P., 1990. The northern Oman Tethyan continental margin:
868 stratigraphy, structure, concepts and controversies. In: Robertson, A.H.F., Searle, M.P., Ries,
869 A.C., (Eds.), *The Geology and Tectonics of the Oman Region*. Geological Society Special
870 Publication No. 49, pp. 3-25.

871

872 Robertson, A.H.F., 1998. Rift-related sedimentation and volcanism of the north-Indian
873 margin inferred from a Permian-Triassic exotic block at Lamayuru, Indus suture zone
874 (Ladakh Himalaya) and regional comparisons. *Journal of Asian Earth Sciences* 16, 159-172.

875

876 Saidi, A., Brunet, M.F., Ricou, L.E., 1997. Continental accretion of the Iran Block to
877 Eurasia as seen from the Late Paleozoic to Early Cretaceous subsidence curves. *Geodinamica*
878 *Acta* 10, 189-208.

879

880 Saunders, A.D., Storey, M., Kent, R.W., Norry, M.J., 1992. Consequences of plume-
881 lithosphere interactions. In: Storey, B.C., Alabaster, T., Pankhurst, R.J. (Eds.), *Magmatism*
882 *and the causes of continental break up*. Geological Society Special Publication No. 68, pp. 41-
883 60.

884

885 Searle, M.P. Lippard, S.J., Smewing, D.J., Rex, D.C. 1980. Volcanic rocks beneath the
886 Semail ophiolite nappe. Geological Society London, 137,589-604

887

888 Searle, M.P., Graham, G.M., 1982. "Oman exotics" - Oceanic carbonate build-ups
889 associated with the early stages of continental rifting. *Geology* 10, 43-49.

890

891 Sharma, M., 1997. Siberian Traps. In Mahoney J., Coffin M.F. (eds), *Large igneous*
892 *provinces: Continental oceanic and planetary flood volcanism*. American Geophysical Union
893 *Geophysical Monograph* 100, 273-295.

Shaw, J.E., Baker, J.A., Kent, A.J.R., Ibrahim, K.M., Menzies, M.A., 2007. The Geochemistry of the Arabian Lithospheric Mantle: a Source for Intraplate Volcanism? *Journal of Petrology* 48, 1495-1512.

Stampfli, G.M., Marcoux, J., Baud, A., 1991. Tethyan margins in space and time. *Paleogeography Paleoclimatology Paleoecology* 87, 373-409.

Stampfli, G.M., Borel, G.D., 2002. A plate tectonic model for the Paleozoic and Mesozoic constrained by dynamic plate boundaries and restored synthetic oceanic isochrons. *Earth Planetary Science Letters* 196, 17-33.

Stein, M., Goldstein, S. L., 1996. From plume head to continental lithosphere in the Arabian-Nubian shield. *Nature* 382, 773-778.

Stern, R.J., 1994. Arc assembly and continental collision in the Neoproterozoic east african orogen: implications for the consolidation of Gondwanaland. *Annual Revue of Earth Planetary Science Letters* 22, 319-351.

Stoeser, D.B., Frost, C.D., 2006. Nd, Pb, Sr, and O isotopic characterization of Saudi Arabian Shield terranes. *Chemical Geology* 226, 163-188.

Sun, S.S., McDonough, W.F., 1989. Chemical and isotopic systematics of oceanic basalts: implication for mantle composition and processes. In: Saunders, A.D., Norry, M.J. (Eds.), *Magmatism in the Ocean Basins*. Geological Society Special Publication 42, pp. 313-345.

Vrielynck, B., Bouysse, P., 2001. Le visage changeant de la Terre. L'éclatement de la Pangée et la mobilité des continents au cours des derniers 250 millions d'années. Publication de la Commission de la Carte Géologique du Monde, Paris, 32 p.

Watts, K.F., 1990. Mesozoic carbonate slope facies marking the Arabian platform margin in Oman: depositional history, morphology and palaeogeography. In: Robertson, A.H.F., Searle, M.P., Ries, A.C. (Eds.), *The Geology and Tectonics of the Oman Region*. Geological Society Special Publication 49, pp. 127-138.

Whitehouse, M.J., Windley, B.F., Stoesser, D.B., Al-Khirbash, S., Mahfood, A.O., Bttat, Haider, A., 2001. Precambrian basement character of Yemen and correlations with Saudi Arabia and Somalia. *Precambrian Research* 105, 357–369.

Willbold, M., Stracke, A., 2006. Trace element composition of mantle end-members: implications for recycling of oceanic and upper and lower continental crust. *Geochemistry Geophysics Geosystems* 7, Q04004, doi:10.1029/2005GC001005.

Wilson M., 1989. *Igneous petrogenesis, a global tectonic approach*. Chapman and Hall publishers, London.

Winchester, J.A., Floyd, P.A., 1977. Geochemical discrimination of different magma series and their different products using immobile elements. *Chemical Geology* 20, 325-343.

Zindler, A., Hart, S.R., 1986. Chemical systematics. *Annual Review of the Earth and Planetary Sciences* 14, 493-571.

Figure captions

Fig. 1. Geological setting. a) The Tethyan Suture (ophiolites and associated mélanges) after Coleman (1981), with locations of the main late Carboniferous, Permian and Triassic volcanic sequences associated to the Neotethyan margins inverted segments (mainly from Garzanti et al., 1999). b) Simplified geological map of the Oman Mountains and associated main structural units (after Glennie et al., 1974). c) Sampling locations on the geological map of the Hawasina nappes (after Béchenec, 1987 modified by de Wever et al., 1990). Sampling sites coordinates of Sinni: 23°25'4''N - 57°09'2''E; Sayjah: 23°11'23''N - 57°51'58''E; Aqil: 22°47'8''N - 57°48'4''E (Om-45); 22°47'2''N - 57°51'3''E (Om-52); 22°47'5''N - 57°48'2''E (Om-42); 22°47'9''N - 57°48'4''E (Om-48 and -49); Jabal Buwaydah 1: 22°53'6''N - 57°05'7''E; Jabal Buwaydah 2: 23°00'8''N - 57°00'E. d) Regional cross section according to Béchenec (1987).

Fig. 2. Selected major element plots for the Triassic Hawasina basin lavas. a) MgO (wt.%), b) TiO₂ (wt.%) and c) Na₂O+K₂O (wt.%) *versus* SiO₂ (wt.%) plots. The trend separating alkaline and tholeiitic fields in c) is from MacDonald and Katsura (1964) and the lava nomenclature from Le Bas et al. (1986).

965

966 Fig. 3. Chondrite and primitive mantle-normalized trace elements patterns of (a) Umar
967 Group samples. b) Comparison between multielement patterns of selected Kawr and Alridh
968 Groups basalts and trachybasalts with OIB patterns and the compositional field of the alkaline
969 Umar Group samples from the Al Qurti UmV₁ unit and the Sinni village (grey array).
970 Chondrite, primitive mantle and OIB compositions are from Sun and McDonough (1989).

971

972 Fig. 4. a) Zr/Ti *versus* Nb/Y discriminating diagram of Winchester and Floyd (1977). b)
973 Plot of Triassic Hawasina basalts and trachybasalts in the Nb/Y *versus* Zr/Y diagram of Fitton
974 et al. (1997) together with Iceland plume-related picritic, tholeiitic and alkaline primary
975 basalts (MgO > 8 wt.%) of the Neo-Volcanic Zone, and the Kolbeinsey and Reykjanes ridge
976 basalts (Kokfelt et al., 2006). Note the deviation towards low Nb/Y values for samples with
977 La/Nb < 1.

978

979 Fig. 5. Initial Pb and Nd isotopic compositions of Triassic Hawasina lavas. Plots of a)
980 (²⁰⁷Pb/²⁰⁴Pb)_i, b) (²⁰⁸Pb/²⁰⁴Pb)_i and c) εNdi against (²⁰⁶Pb/²⁰⁴Pb)_i. The compositional fields of
981 Indian and Atlantic MORB are compiled from the Petrological Database of the Ocean Floor
982 (PETDB). Compositional fields of OIB, mantle isotopic components HIMU (for High-μ), EM
983 1 and EM 2 (for Enriched Mantle 1 and 2) and the NHRL (Northern Hemisphere Reference
984 Line) are from Zindler and Hart (1986).

985

986 Fig. 6. a) and b) Al₂O₃ (wt.%) and Eu/Eu* *versus* SiO₂ (wt.%) diagrams for Al Qurti
987 samples of the Umar Group c) (La/Yb)_N ratios of Al Qurti samples plotted against their
988 stratigraphic position. d) and e) (La/Yb)_N *versus* La(ppm) and εNd_i *versus* SiO₂ (wt.%)
989 diagrams for all Triassic Hawasina samples.

990

991 Fig. 7. Selected REE plots. a) and b) (La/Yb)_N and La *versus* (Sm/Yb)_N plots for
992 Hawasina Triassic basalts and trachybasalts. The meaning of arrows (1) and (2) is explained
993 in the text. c) La/Yb and Yb (ppm) variations during non-modal partial melting (F values:
994 partial melting degrees) of garnet and spinel lherzolite sources “s” containing different
995 proportions of these minerals (100% Gt – 0% Sp, 50 % - 50 %, 30% - 70%, 0% Gt – 100%
996 Sp). In this model developed by Luhr et al. (1995), source “s” is assumed to be enriched
997 relative to chondrite, with La = 6 * Ch (1.79 ppm) and Yb = 1.5 * Ch (0.31 ppm). This model
998 was used by Luhr et al. (1995) for primitive basalts with Mg# > 68 to limit the fractionation
999 effects related to magmatic differentiation. As the iron contents of the studied basalts may
1000 have been modified by post-magmatic processes, their MgO contents are used to check the

primitive character Hawasina Triassic basalts. Samples with $\text{MgO} > 7$ wt.% are identified by thick and doubled symbols.

Fig. 8. Plots of the ϵNd_i of Triassic Hawasina basalts and trachybasalts against: a) La/Nb ; b) Th/Nb ; c) $(\text{La/Sm})_N$ and d) Ti/Y . MORB and OIB compositions are from Sun and McDonough (1989). SCLM (Sub-Continental Lithospheric Mantle) composition is from McDonough (1990) and the compositions of LC and UC (Lower and Upper continental Crust) from McLennan (2001).

Fig. 9. Nd and Pb isotopic compositions of Triassic Hawasina volcanics recalculated at $t = 230$ My, compared to the published fields of the Arabian sub-continental lithospheric mantle and the regional upper and lower crusts. E. Pr.: Early Proterozoic, Ar: Archean, L. Ar.: Late Archean. MORB, OIB, EM 1 and EM 2 are from Zindler and Hart (1986); NHRL is from Hart (1984); Arabian lithospheric mantle is from Shaw et al. (2007 - Jordan), Baker et al. (2002, 1997 - Yemen and Southern Red Sea), Hamelin and Allègre (1988 - Zabargad Island), Blusztajn et al. (1995 - Saudi Arabia). Sudanese crust is from Davidson and Wilson (1989); Yemen and Saudi Arabia upper crust is from Whitehouse et al. (2001); Baker et al. (2000); Hegner and Pallister (1989); the lower mafic crust is from Cohen et al. (1984 - Tanzania), Altherr et al. (1990) and G. Chazot and J. A. Baker (unpublished data presented as a composition field in Baker et al., 1997 - Arabia and Yemen); the gneissic lower crust is from Lancelot and Bosch (1991 - Zabargad Island).

Fig. 10. Nd and Pb isotopic compositions (at $t = 230$ My) of Triassic intraplate volcanic sequences from Oman and the Eastern Mediterranean occurrences. Data are from this work (Oman); Lapierre et al., 2007 (Cyprus); Maury et al., 2008 (Turkey); Perez, 2006 (Syria); Monjoie et al., 2008 (Greece).

Fig. 11. Geochemical comparison between the Permian and Triassic lavas from the Oman margin. All Permian data are from Lapierre et al. (2004) and Maury et al. (2003). a) and b) plots of TiO_2 (wt.%) and $(\text{La/Sm})_N$ versus Th (ppm) for basalts from the two magmatic events. c) Primitive mantle-normalized multielement patterns of the Permian Groups 1, 2 and 3 and of the Triassic basalts and trachybasalts.

Fig. 12. a) and b) Plots of $\epsilon(\text{Nd})_i$ values versus $(\text{La/Sm})_N$ and La/Nd ratios for the Permian Groups 1, 2 and 3 (Lapierre et al., 2004) and the Triassic basalts and trachybasalts. c) $\epsilon(\text{Nd})_i$ versus $(^{206}\text{Pb}/^{204}\text{Pb})_i$ diagrams. All isotopic data are recalculated at $t = 230$ My. The meaning

of A, B, C and D in diagrams a) and b) is explained in the text. MORB, OIB and primitive mantle reference values are from Sun and McDonough (1989).

Table captions

Table 1. Major element (wt.%) and trace element (ppm) compositions of representative Triassic lavas (whole set shown in Appendix A). Trace element compositions measured by ICP-AES are shown in italics and those obtained by ICP-MS in normal numbers. B: basalts ($\text{SiO}_2 < 53$ wt.% and $\text{MgO} > 6$ wt.%); TB: trachybasalts ($\text{SiO}_2 < 53$ wt.% and $\text{MgO} = 3$ to 6 wt.%); DB: basaltic dolerite; TA: trachyandesite; T: trachyte; R: Rhyolite. Analytical methods explained in the text.

Table 2. Nd and Pb actual and initial (“i” for $t = 230$ My) isotopic compositions with their uncertainties ($\pm 2 \sigma$) for Triassic volcanics from the Hawasina nappes. Analytical methods explained in the text.

Appendix

Appendix A. Selected sampling sites. a) Cross section and sample locations in the Al Qurti site of the Umar Group (Fig. 1c). b) Stratigraphic column of the basal 300 m of the Kawr Group at Jabal Misfah (Fig. 1c) and location of samples.

Appendix B. Major element and trace element compositions of Triassic lavas from the Hawasina Nappes. Trace element compositions measured by ICP-AES are shown in italics and those obtained by ICP-MS in normal numbers. B: basalts ($\text{SiO}_2 < 53$ wt.% and $\text{MgO} > 6$ wt.%); TB: trachybasalts ($\text{SiO}_2 < 53$ wt.% and $\text{MgO} > 3$ wt.%); DB: basaltic dolerite; TA: trachyandesite; T: trachyte; R: Rhyolite. Analytical methods explained in the text.

Appendix C. Chondrite and primitive mantle-normalized trace elements patterns of Middle to Late Triassic lavas from the Hawasina Nappes. Chondrite and primitive-mantle compositions are from Sun and McDonough (1989).

Appendix D. Plots of La, Nd, Sm, U and Pb against Th (ppm) for Triassic Hawasina samples. The linear trends reported on some diagrams correspond to the average Th/U and Th/Pb ratios of OIB (Sun and McDonough, 1989).

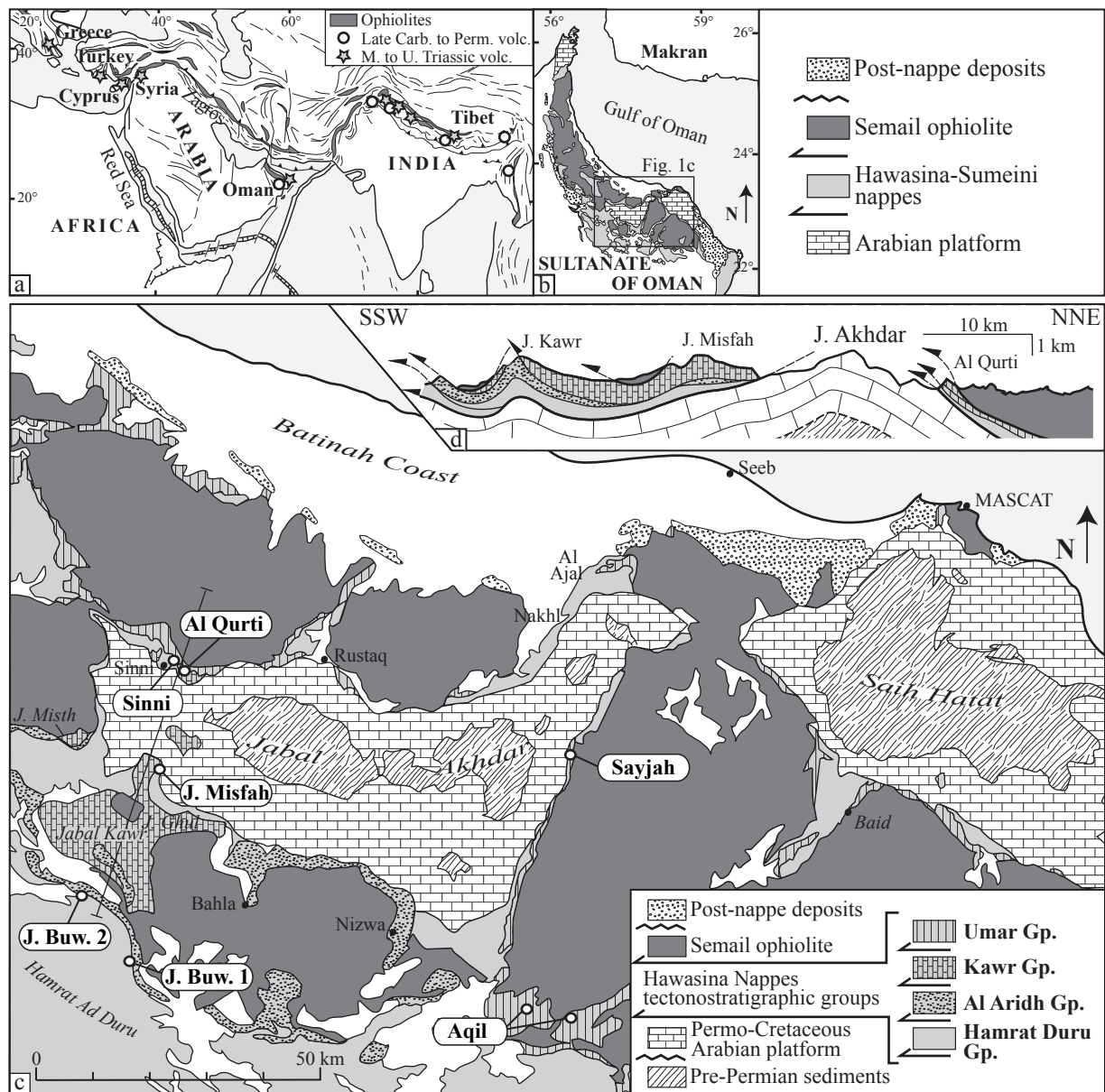


Fig. 1

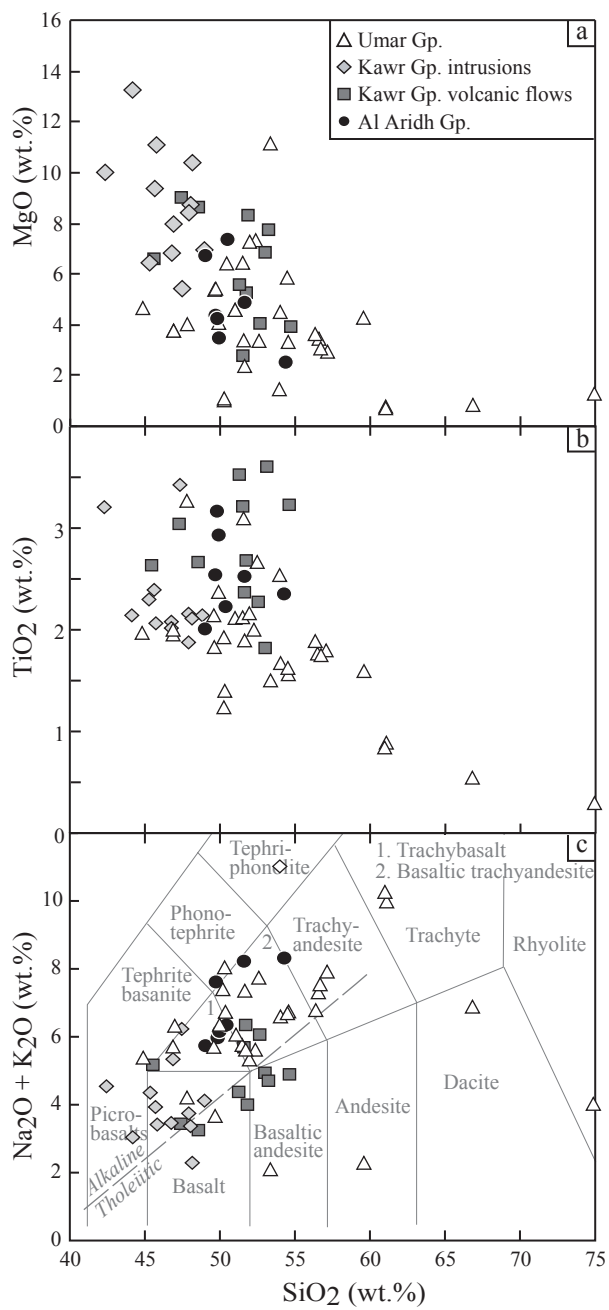


Fig. 2

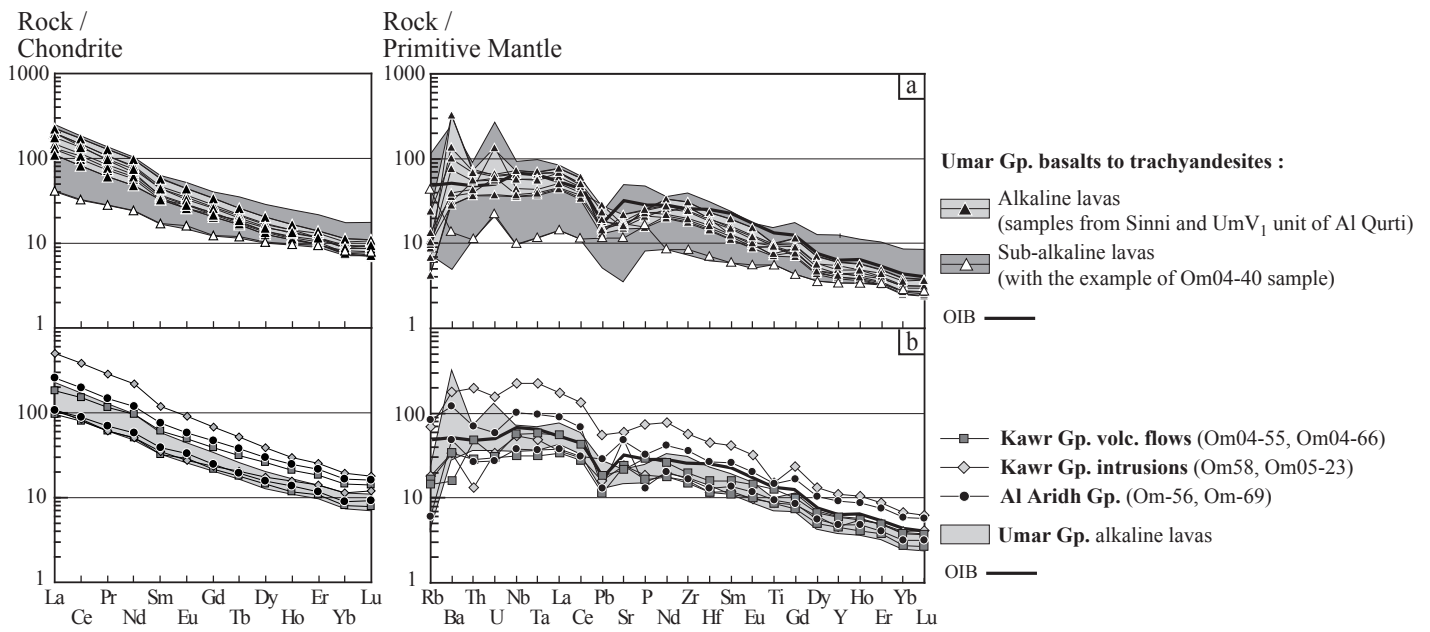


Fig. 3

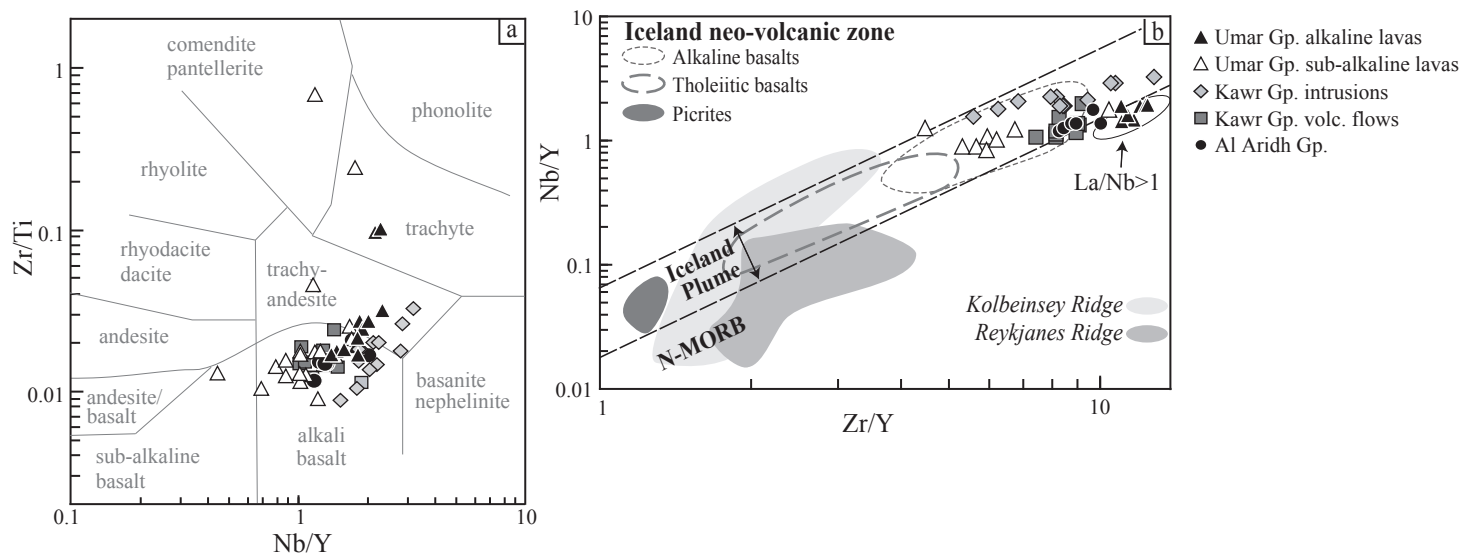


Fig. 4

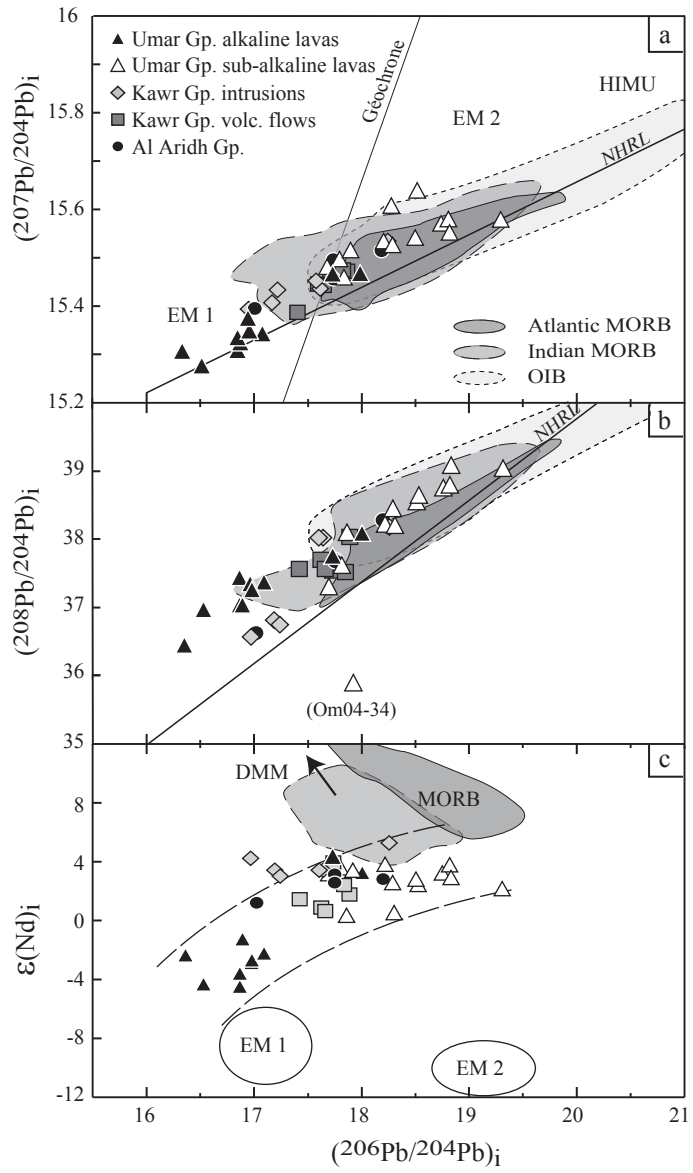


Fig. 5

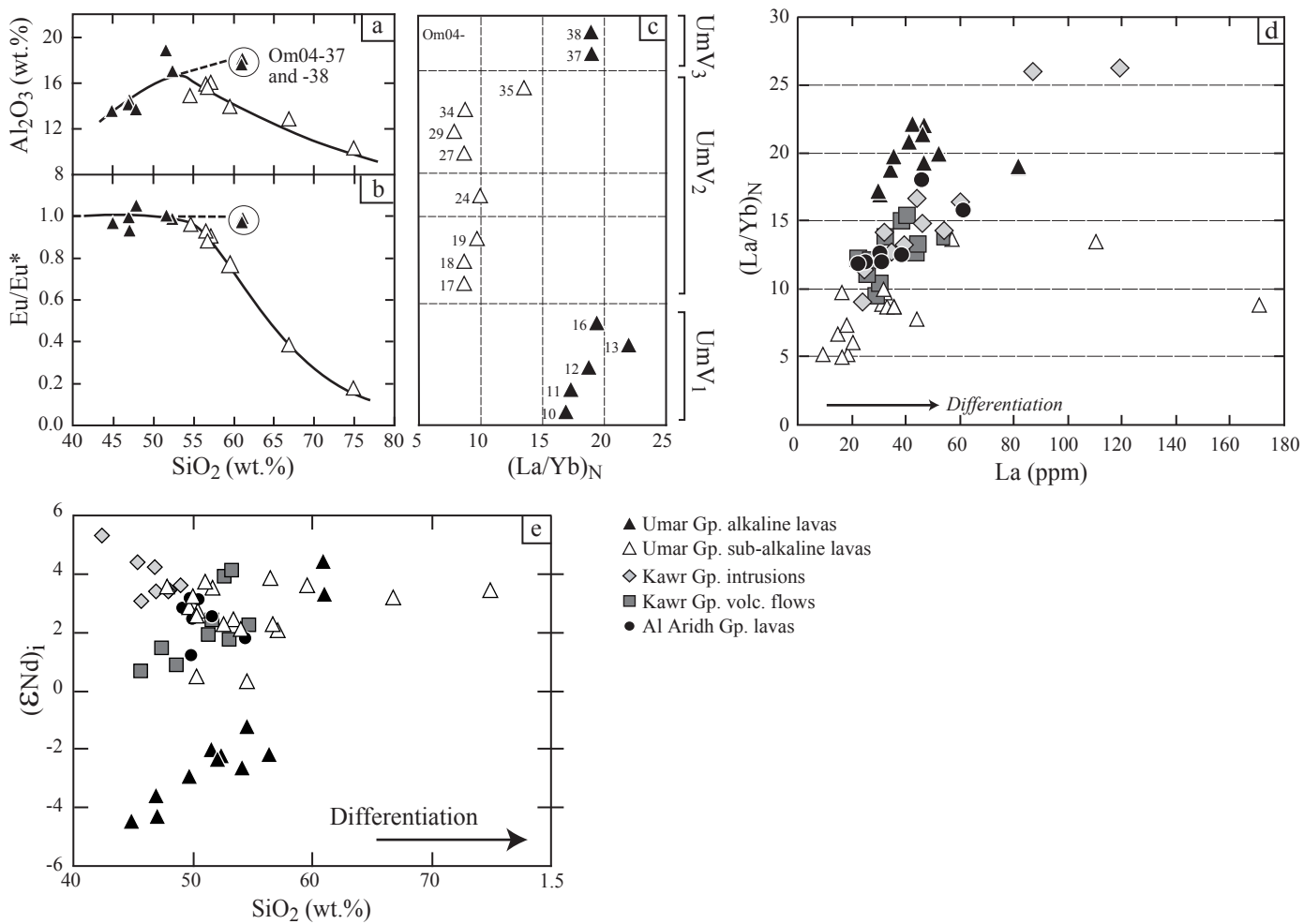


Fig. 6

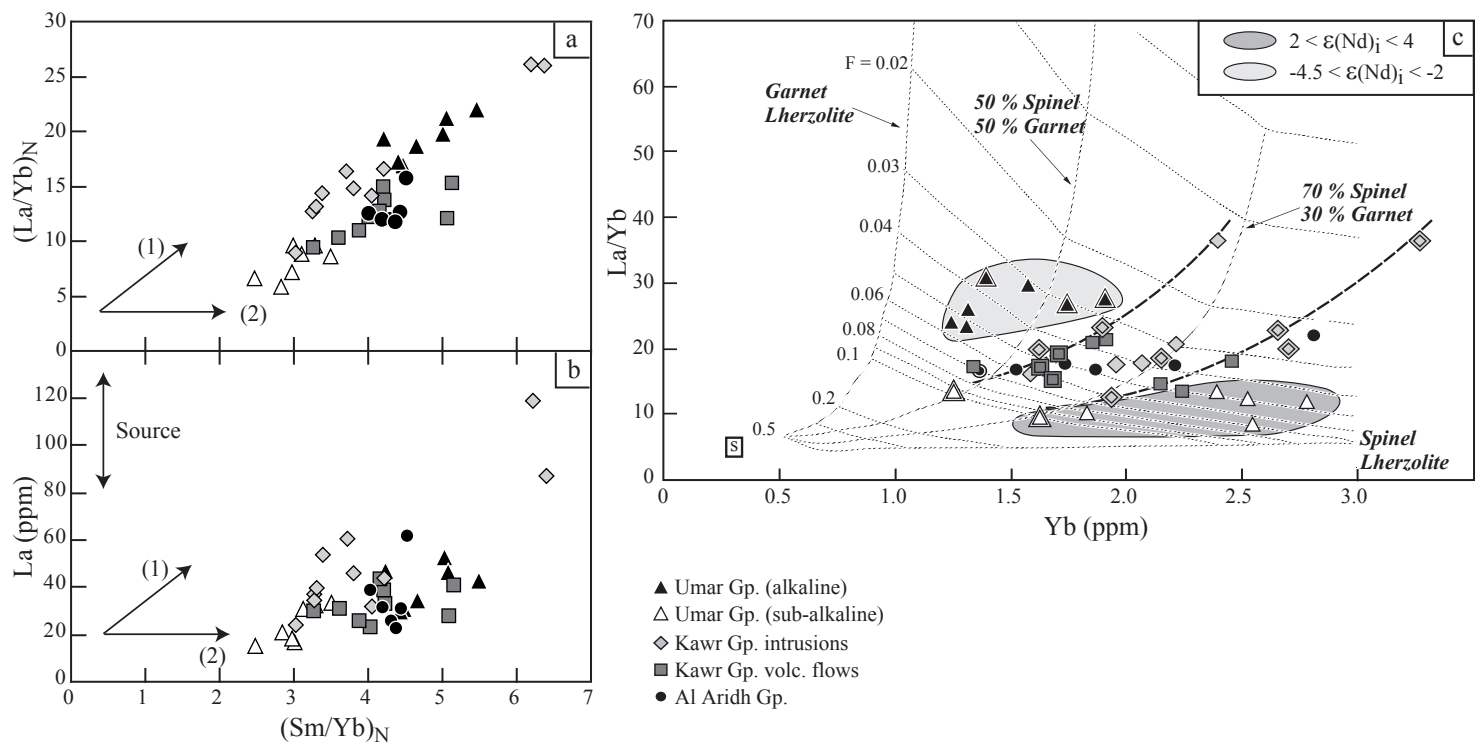


Fig. 7

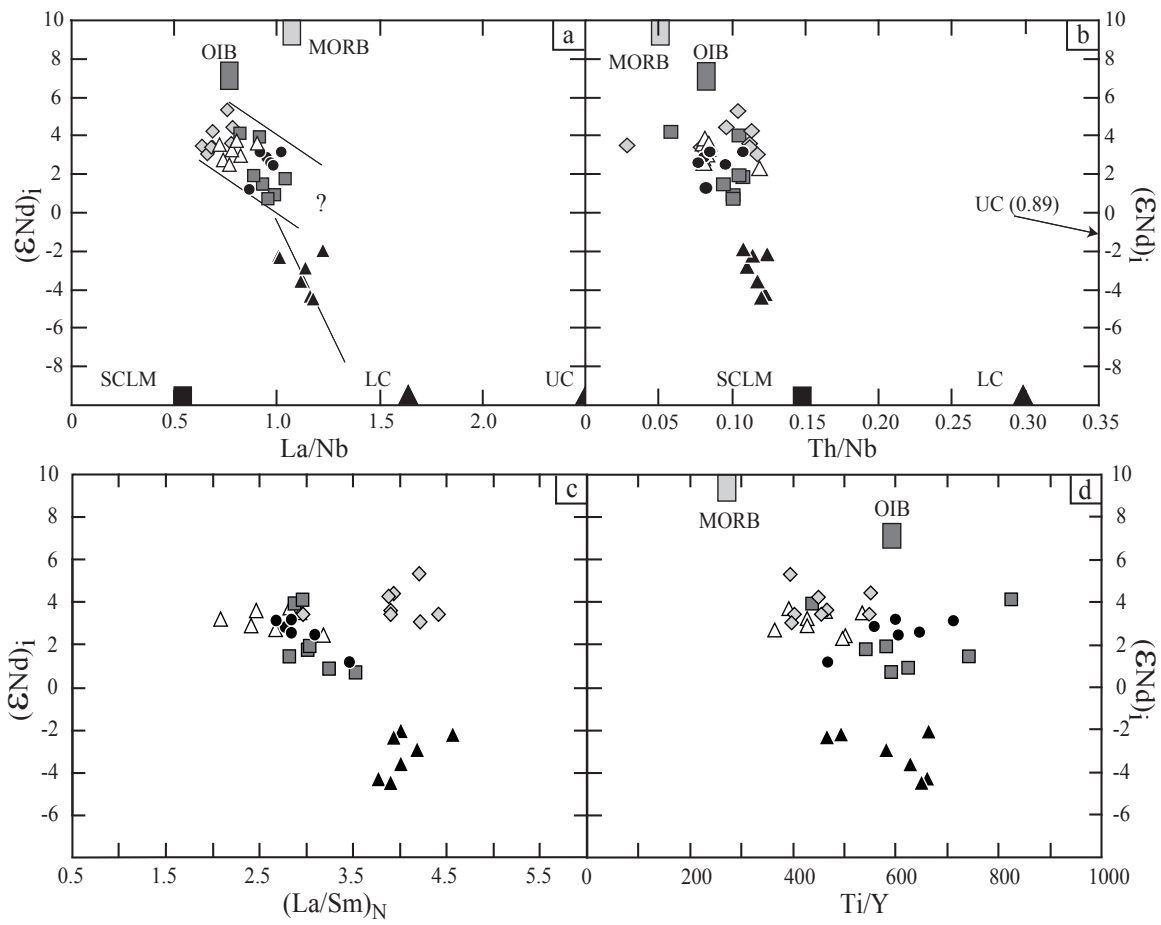


Fig. 8

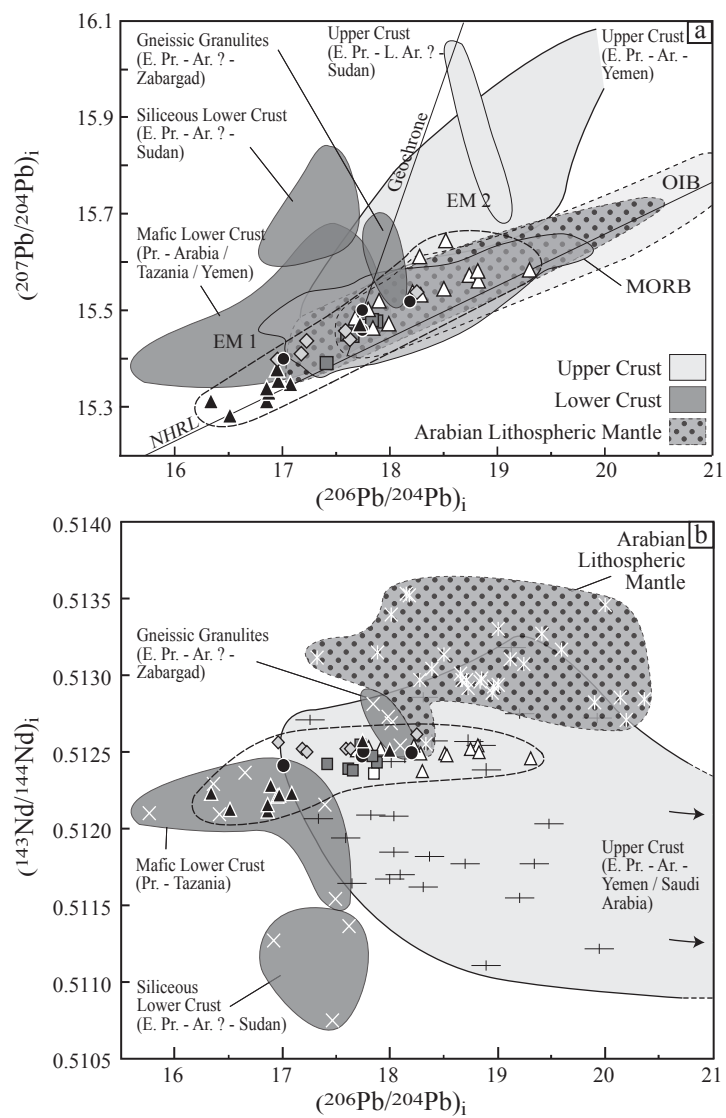


Fig. 9

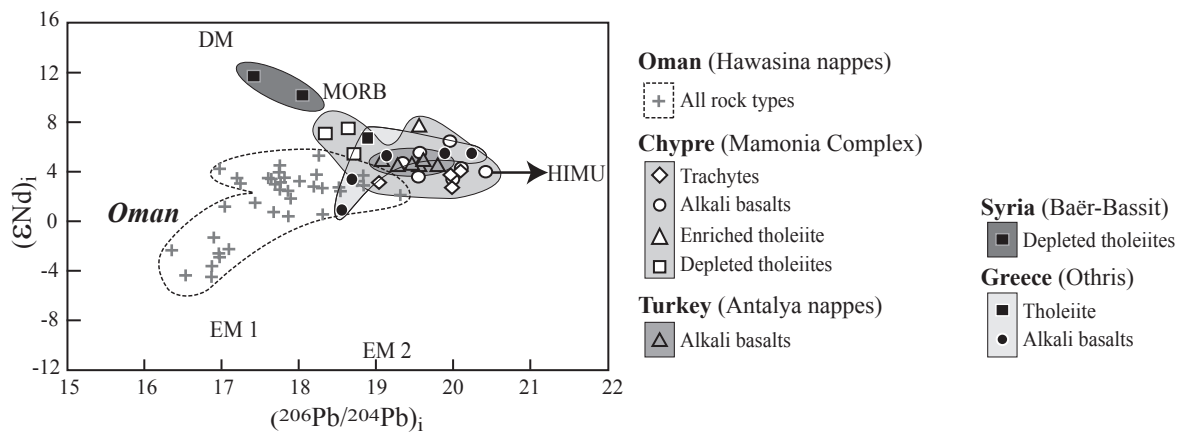


Fig. 10

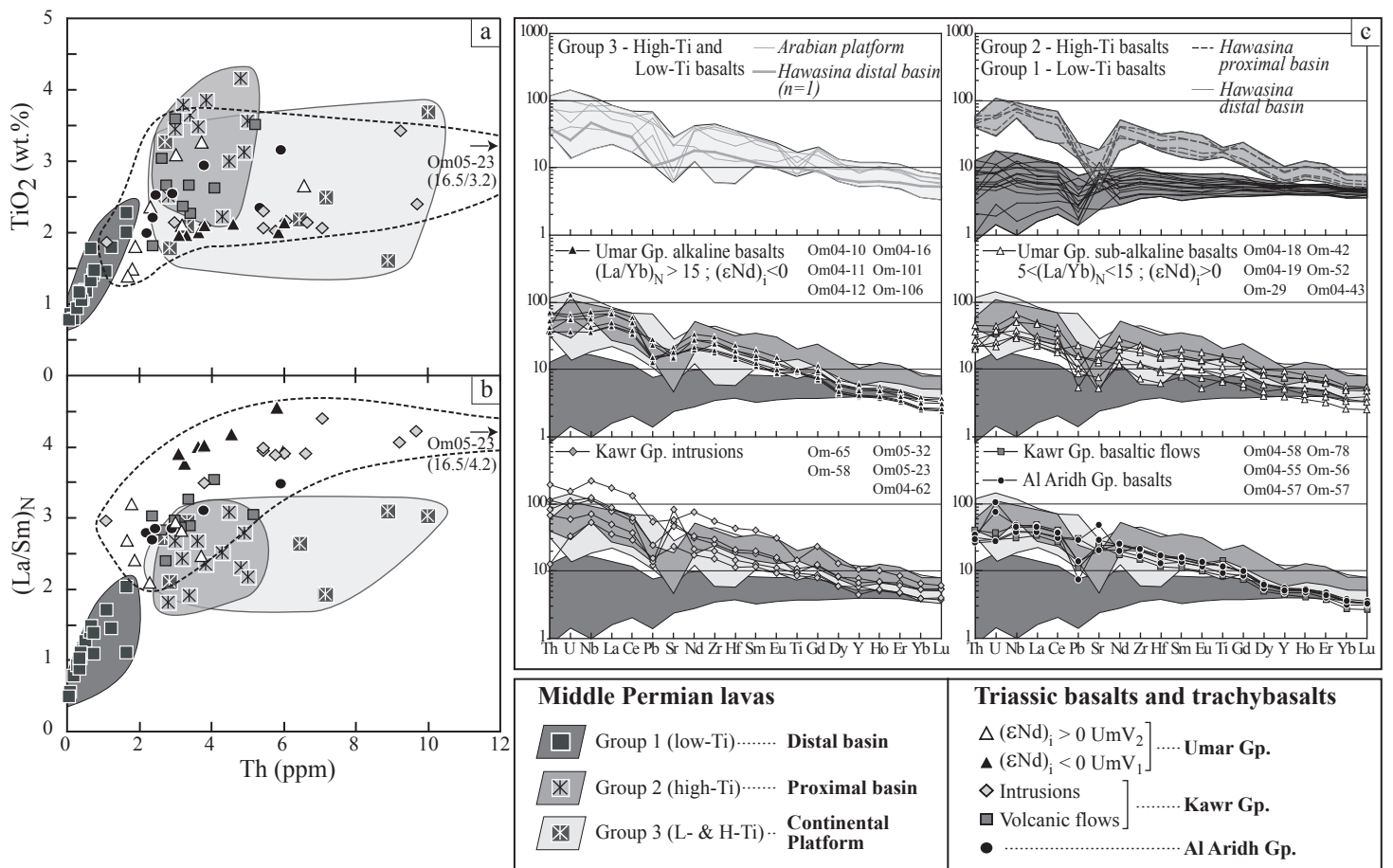


Fig. 11

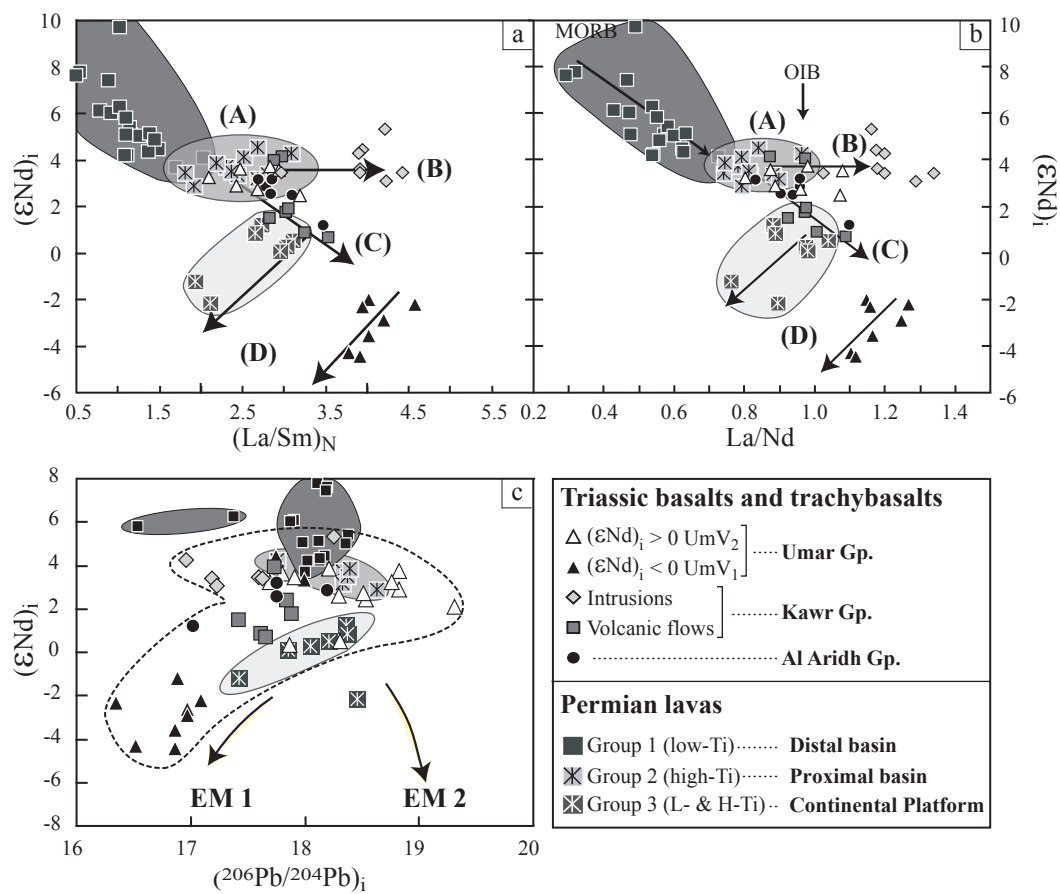


Fig. 12

Table 1

Stratigraphic Gp. and position	Umar Group - Sinni Fm.									Kawr Group - Misfah Fm.			
	UmV ₁ alkaline lavas					UmV ₂ sub-alkaline lavas				Volcanic Flows		Intrusions	
Location	Al Qurti			Sinni		Al Qurti			Sayjah	Jabal Misfah			
Samples	Om04-11	Om04-13	Om04-16	Om-101	Om-106	Om04-24	Om04-29	Om 04-35	Om04-40	Om04-55	Om 04-57	Om- 58	Om05-23
Rock Type	TB	TA	BD	B	TB	TA	TA	R	TA	B	B	B	B
Major Elements (wt. %) recalculated on a volatile-free basis													
SiO ₂	44.9	54.6	52.4	52.0	49.7	56.5	59.6	66.8	50.3	53.1	48.6	48.0	42.4
TiO ₂	1.96	1.57	2.01	2.14	2.13	1.77	1.59	0.54	1.22	1.81	2.65	1.87	3.21
Al ₂ O ₃	13.6	14.9	17.0	15.2	14.8	15.9	13.9	12.9	15.1	14.8	15.0	16.2	12.7
Fe ₂ O ₃	9.88	5.81	9.14	9.61	8.81	8.38	12.27	6.07	7.68	11.93	9.37	12.01	15.84
MnO	0.13	0.11	0.16	0.14	0.14	0.11	0.14	0.29	0.10	0.22	0.19	0.13	0.25
MgO	4.66	3.31	7.35	7.21	5.38	3.41	4.25	0.83	1.02	6.85	8.63	8.75	10.00
CaO	19.08	12.48	5.79	7.87	12.83	5.88	5.34	5.48	16.83	6.02	11.79	9.29	9.47
Na ₂ O	4.95	6.41	4.36	4.47	5.43	6.67	0.35	5.30	5.96	4.36	2.83	2.66	1.39
K ₂ O	0.43	0.34	1.23	0.78	0.22	0.64	1.92	1.56	1.40	0.56	0.37	0.68	3.10
P ₂ O ₅	0.45	0.50	0.55	0.53	0.53	0.70	0.67	0.22	0.35	0.35	0.52	0.40	1.58
Vol.-free total*	99.93	99.66	99.44	99.69	99.68	99.17	99.22	99.42	100.03	99.59	99.91	99.49	99.52
LOI	10.82	9.15	5.30	3.99	6.15	5.44	2.85	7.54	12.09	3.17	4.47	7.45	4.51
Trace elements (ppm)													
Sc	20	11	19	33	28	20	13	1	22	34	36	10	18
V	220	142	190	283	235	99	33	7	93	220	190	105	99
Ni	107	45	105	185	187	205	4	5	56	191	164	235	128
Co	32	18	31	46	41	29	17	3	18	44	44	59	39
Cr	200	64	161	355	400	162	2	4	190	454	385	300	155
Cs	0.17	0.09	0.61	0.37	0.18	0.40	0.24	0.46	1.74	0.17	0.06	0.18	0.98
Rb	6.2	4.3	15.2	6.7	2.7	11.1	29.7	18.0	27.0	10.1	2.8	11.5	43.1
Ba	198	2293	701	943	218	84	195	418	93	235	393	235	1243
Th	3.10	6.40	5.84	6.01	4.58	4.12	6.58	16.06	0.92	2.39	3.40	1.10	16.54
U	0.78	1.34	1.27	1.37	1.17	0.87	1.65	2.69	0.46	0.62	0.78	0.70	3.24
Nb	25.59	47.52	46.68	51.82	41.03	36.51	64.31	136.66	6.85	21.92	33.19	38.26	157.63
Ta	1.51	2.75	2.65	2.84	2.29	2.28	3.54	7.88	0.47	1.26	2.01	1.96	9.10
Pb	2.63	3.33	4.33	2.39	2.80	3.28	3.11	5.29	2.14	2.05	2.44	2.88	10.10
Sr	364	353	315	463	384	271	74	200	244	492	504	500	1237
Zr	200	302	295	346	273	190	437	783	93	164	232	174	630
Hf	4.43	5.94	6.05	7.20	5.92	4.34	9.37	17.12	2.15	3.55	5.04	3.56	13.60
Y	18.09	20.17	24.43	27.59	21.94	28.96	55.27	75.70	15.28	20.03	25.36	20.47	49.01
La	30.01	46.54	47.10	52.69	46.74	31.75	44.46	110.67	9.65	22.79	32.84	24.28	119.00
Ce	59.51	84.53	89.88	105.22	88.64	63.08	95.92	221.24	19.97	47.95	70.31	51.87	233.93
Pr	6.95	9.03	10.14	12.17	9.97	7.26	11.83	25.31	2.65	5.79	8.21	5.81	27.34
Nd	26.90	31.97	37.16	45.45	37.49	28.33	47.37	93.56	11.33	23.39	32.60	23.71	102.62
Sm	4.96	5.52	6.65	8.62	7.20	5.99	10.37	17.76	2.61	4.87	6.51	5.28	18.23
Eu	1.49	1.63	2.00	2.56	2.10	1.82	2.61	2.08	0.93	1.65	2.06	1.60	5.26
Gd	4.22	4.65	5.40	6.81	5.71	5.79	10.01	14.49	2.55	4.38	5.54	4.83	13.83
Tb	0.61	0.66	0.79	0.96	0.80	0.93	1.63	2.31	0.44	0.66	0.83	0.77	1.93
Dy	3.23	3.48	4.23	5.15	4.32	5.34	9.09	12.77	2.61	3.61	4.56	4.41	9.70
Ho	0.61	0.67	0.80	0.94	0.80	1.04	1.79	2.46	0.55	0.66	0.85	0.89	1.68
Er	1.58	1.82	2.13	2.32	1.94	2.86	4.82	6.63	1.57	1.78	2.16	2.31	4.17
Yb	1.25	1.52	1.75	1.91	1.58	2.29	4.09	5.88	1.37	1.34	1.71	1.94	3.27
Lu	0.18	0.23	0.27	0.28	0.23	0.33	0.61	0.83	0.20	0.20	0.24	0.30	0.46

* : Volatile-free total (not recalculated to 100%)

Table 2

	$^{143}\text{Nd}/^{144}\text{Nd}$	$^{147}\text{Sm}/^{144}\text{Nd}$	$(^{143}\text{Nd}/^{144}\text{Nd})_i$	$\epsilon\text{Nd}(t)$	$^{206}\text{Pb}/^{204}\text{Pb}$		$^{207}\text{Pb}/^{204}\text{Pb}$		$^{208}\text{Pb}/^{204}\text{Pb}$	
					Measured	Initial	Measured	Initial	Measured	Initial
Umar Group - Sinni Fm. - Al Qurti										
Om04-10	0.512294 ± 8	0.114	0.51212	-4.29	17.4943 ± 4	16.52	15.3298 ± 4	15.28	37.8082 ± 1.2	36.96
Om04-11	0.512282 ± 15	0.112	0.51211	-4.45	17.5206 ± 5	16.86	15.3451 ± 6	15.31	37.9099 ± 1.5	37.05
Om04-11 dup.	0.512317 ± 8		0.51215			16.86		15.31		37.05
Om04-12	0.512329 ± 8	0.113	0.51216	-3.58	18.0601 ± 5	16.86	15.3981 ± 7	15.34	37.9644 ± 1.7	37.45
Om04-13	0.512437 ± 9	0.104	0.51228	-1.21	17.7923 ± 8	16.89	15.3738 ± 8	15.33	38.4578 ± 2.4	37.04
Om04-16	0.512392 ± 34	0.108	0.51223	-2.20	17.7423 ± 6	17.08	15.3805 ± 5	15.35	38.3722 ± 1.4	37.38
Om04-17	0.512644 ± 6	0.130	0.51245	2.08						
Om04-18	0.512734 ± 8	0.138	0.51253	3.59						
Om04-19	0.512739 ± 5	0.143	0.51252	3.54						
Om04-24	0.512732 ± 8	0.128	0.51254	3.86	18.8267 ± 7	18.21	15.5678 ± 7	15.54	39.1755 ± 2.2	38.23
Om04-27	0.512651 ± 6	0.127	0.51246	2.30						
Om04-29	0.512726 ± 5	0.132	0.51253	3.61	19.0324 ± 6	17.80	15.5617 ± 5	15.50	39.2381 ± 1.5	37.63
Om04-34	0.512692 ± 8	0.115	0.51252	3.45	18.7785 ± 15	17.91	15.5614 ± 13	15.52	41.0226 ± 3.8	35.91
Om04-35	0.512679 ± 6	0.115	0.51251	3.21	18.8748 ± 7	17.69	15.5437 ± 12	15.48	39.6130 ± 1.8	37.30
Om04-37	0.512668 ± 9	0.103	0.51251	3.34	18.7146 ± 6	18.00	15.5079 ± 6	15.47	38.9815 ± 1.6	38.10
Om04-37 dup.	0.512644 ± 8		0.51249							
Om04-38	0.512726 ± 4	0.104	0.51257	4.44	19.0516 ± 9	17.74	15.5368 ± 7	15.47	39.2490 ± 2.9	37.71
Umar Group - Sinni Fm. - Sayjah										
Om04-40	0.512578 ± 9	0.139	0.51237	0.52	18.7916 ± 8	18.30	15.5522 ± 11	15.53	38.5080 ± 3.1	38.19
Om04-42	0.512671 ± 9	0.130	0.51247	2.59	18.9639 ± 6	18.29	15.6414 ± 7	15.61	39.0166 ± 2.5	38.42
Om04-43	0.512665 ± 9	0.131	0.51247	2.45	18.8248 ± 7	18.53	15.6553 ± 7	15.64	38.9572 ± 1.9	38.63
Umar Group - Sinni Fm. - Aqil										
Om-42	0.512705 ± 10	0.143	0.51249	2.88	19.5056 ± 38	18.83	15.5908 ± 83	15.56	40.0108 ± 8.3	39.09
Om-45	0.512737 ± 12	0.135	0.51253	3.73	19.4132 ± 5	18.82	15.6080 ± 16	15.58	39.6322 ± 1.6	38.78
Om-48	0.512621 ± 11	0.107	0.51246	2.30						
Om-49	0.512630 ± 12	0.119	0.51245	2.12	22.9014 ± 41	19.31	15.7637 ± 73	15.58	40.5965 ± 7.3	39.03
Om-52	0.512693 ± 13	0.140	0.51248	2.74	19.1322 ± 11	18.51	15.5731 ± 25	15.54	38.9681 ± 2.5	38.53
Umar Group - Sinni Fm. - Sinni										
Om-29	0.512733 ± 9	0.150	0.51251	3.23	19.6348 ± 11	18.76	15.6148 ± 33	15.57	39.6663 ± 3.3	38.74
Om-97	0.512560 ± 10	0.133	0.51236	0.34	18.4306 ± 11	17.86	15.4878 ± 38	15.46	39.0129 ± 3.5	38.09
Om-99	0.512380 ± 10	0.115	0.51221	-2.63	17.7599 ± 11	16.97	15.3899 ± 43	15.35	38.2116 ± 4.3	37.25
Om-100	0.512406 ± 10	0.111	0.51224	-2.02						
Om-101	0.512395 ± 8	0.115	0.51222	-2.33	17.6334 ± 7	16.35	15.3730 ± 22	15.31	38.2907 ± 2.2	36.45
Om-106	0.512368 ± 7	0.116	0.51219	-2.90	17.9091 ± 6	16.97	15.4220 ± 20	15.37	38.5366 ± 2	37.33
Om-107	0.512397 ± 8	0.110	0.51223	-2.15						
Kawr Group - Misfah Fm. - Jabal Misfah volcanic flows										
Om04-52	0.512740 ± 3	0.131	0.51254	3.92	18.4416 ± 16	17.73	15.5010 ± 5	15.46	38.6140 ± 0.6	37.54
Om04-55	0.512621 ± 4	0.126	0.51243	1.75	18.5782 ± 8	17.88	15.5096 ± 9	15.47	38.9022 ± 1.7	38.03
Om04-56	0.512652 ± 4	0.125	0.51246	2.40	18.3903 ± 18	17.85	15.5036 ± 5	15.48	38.7267 ± 0.6	37.51
Om04-57	0.512569 ± 2	0.121	0.51239	0.88	18.3430 ± 7	17.62	15.4823 ± 11	15.45	38.7372 ± 0.6	37.70
Om04-58	0.512609 ± 4	0.128	0.51242	1.46	18.0598 ± 9	17.42	15.4213 ± 7	15.39	38.4593 ± 2	37.55
Om04-58 dup.					18.0597 ± 11		15.4220 ± 11		38.4589 ± 2.8	
Om04-63	0.512558 ± 6	0.120	0.51238	0.67	18.1177 ± 15	17.66	15.4658 ± 5	15.44	38.4996 ± 0.6	37.56
Om04-63 dup.	0.512568 ± 4		0.51239		18.1186 ± 16		15.4666 ± 5		38.5041 ± 0.5	
Om04-66	0.512629 ± 3	0.125	0.51244	1.92						
Om-207	0.512649 ± 7	0.127	0.51246	2.26						
Om-66	0.512725 ± 12	0.114	0.51255	4.11						
Kawr Group - Misfah Fm. - Jabal Misfah intrusions										
Om-58	0.512721 ± 15	0.135	0.51252	3.44	18.1451 ± 7	17.60	15.4832 ± 17	15.46	38.3142 ± 1.7	38.03
Om-61	0.512705 ± 9	0.118	0.51253	3.63						
Om-62	0.512743 ± 10	0.116	0.51257	4.42						
Om-65	0.512696 ± 10	0.119	0.51252	3.43	18.8151 ± 6	17.63	15.4988 ± 15	15.44	39.2059 ± 1.5	38.03
Om04-61	0.512698 ± 6	0.120	0.51252	3.43	18.0065 ± 14	17.18	15.4503 ± 5	15.41	38.1773 ± 0.4	36.82
Om04-62	0.512742 ± 7	0.120	0.51256	4.27	18.0312 ± 16	16.96	15.4503 ± 6	15.40	38.1788 ± 0.7	36.56
Om05-23	0.512776 ± 3	0.107	0.51261	5.32	19.0003 ± 11	18.25	15.5746 ± 3	15.54	39.4324 ± 0.4	38.19
Om05-32	0.512678 ± 5	0.119	0.51250	3.06	19.2816 ± 16	17.23	15.5398 ± 5	15.43	40.0011 ± 0.6	36.74
Al Aridh Group - Sayfam Fm. - Jabal Buwaydah										
Om-56	0.512689 ± 10	0.134	0.51249	2.82	18.4473 ± 7	18.20	15.5283 ± 18	15.52	38.5951 ± 1.8	38.28
Om-56 dup.	0.512703 ± 11		0.51250							
Om-57	0.512659 ± 15	0.124	0.51247	2.54	19.7132 ± 9	17.75	15.5563 ± 20	15.46	38.4000 ± 2	37.67
Om-67	0.512597 ± 12	0.109	0.51243	1.79						
Om-69	0.512589 ± 10	0.124	0.51240	1.19	18.1816 ± 7	17.02	15.4554 ± 23	15.40	38.4655 ± 2.3	36.61
Om-75	0.512645 ± 12	0.118	0.51247	2.45						
Om-78	0.512701 ± 9	0.131	0.51250	3.15	20.4541 ± 10	17.76	15.6349 ± 38	15.50	39.3558 ± 3.8	37.69
Om-80	0.512685 ± 8	0.121	0.51250	3.14						